R. & M. No. 2919
(15,259)
A.R.C. Technical Report

MINISTRY OF SUPPLY

AERONAUTICAL RESEARCH COUNCIL
REPORTS AND MEMORANDA

Effects of Reynolds Number on the Flow of Air through a Cascade of Compressor Blades

By

H. G. RHODEN, M.A., M.Sc.

LONDON: HER MAJESTY'S STATIONERY OFFICE

1956

NINE SHILLINGS NET

Effects of Reynolds Number on the Flow of Air through a Cascade of Compressor Blades

By

H. G. Rhoden, M.A., Wh.Sc.

of University Engineering Department, Cambridge

Communicated by the Principal Director of Scientific Research (Air), Ministry of Supply

Reports and Memoranda No. 2919

June, 1952

1. *Summary.*—The experimental work consisted of the separate testing of three cascades of axial-flow compressor blades of camber angles 20 deg, 30 deg and 40 deg respectively. Measurements were made of the distribution of static pressure over the central cross-section of the middle blade of each cascade, together with traverses of static pressure, total head and angle of flow at inlet and outlet to each cascade in the plane of the central cross-section. The tests covered a range of actual Reynolds number from 3×10^4 to 5×10^5, based on the inlet air velocity and the blade chord, and also a range of inlet air angle α_1, from 35 deg to 60 deg. In the tests there were numerous cases of laminar boundary-layer separation at low Reynolds numbers and a few cases of turbulent separation at higher Reynolds numbers. These occurred on the convex surfaces of the blades. There were also a few cases of laminar separation from the concave surfaces of the blades. The results show the effect of Reynolds number, blade camber, and inlet air angle on cascade performance. The type of pressure distribution likely to give good performance over a wide range of Reynolds number is discussed.

2. *Introduction.*—In axial-flow compressor blade passages separation of the boundary layer from the blade surfaces increases the losses and reduces the pressure rise. Separation of either the laminar or turbulent boundary layers can occur, depending on the Reynolds number at which the passage is operating. The presence of separation can be observed from measurements of static pressure on the blade surfaces. This takes the form of an interruption, at the point of separation, in a positive pressure gradient, the pressure tending to become constant if separation is complete. It can also be observed from traverses of total head across the blade wakes at outlet from the cascade, showing as a broadening of the wakes.

Initially it was decided to test compressor blades in stationary cascades. The tests included the measurement of the distribution of static pressure over the surface of the middle blade of each cascade at the central cross-section, and traverses of static pressure, total head and angle of flow at inlet and outlet to each cascade in the plane of the central cross-section.

The range of Reynolds numbers was chosen so as to be low enough to include, in many cases, those Reynolds numbers at which laminar boundary-layer separation occurs, and to be high enough to cover the practical range of Reynolds number, possibly also including some cases of turbulent boundary-layer separation. Blades of large chord were necessary in order to give a sufficient number of static-pressure tappings, and, for the range of Reynolds numbers covered, to result in compressibility effects being negligible.

It was thought advisable to test blades of a shape and setting which had already been tested in other tunnels, for efficiency and angle of deflection, so that additional evidence would then be available concerning the effects of the tunnel on cascade performance. In consultation with the National Gas Turbine Establishment, it was decided that three blade shapes, suitable for axial-flow compressor blades should each be tested at the same pitch/chord ratio, and at a stagger chosen in each case to give approximately the same outlet air angle α_2. The pitch/chord ratio and the outlet air angle α_2 have a major effect on compressor performance, so that comparisons are best made for fixed values of these quantities. The blade length was sufficient to reduce to a small value the effect of the blade ends on the outlet traverses, taken in the plane of the central cross-section over the middle two or three blades. The tests were carried out over a sufficiently wide range of inlet air angle α_1 to give data on both the positive and negative stalling of the cascades.

3. *Apparatus.*—3.1. *Cascades.*—For the three cascades tested, the data specifying the blade shapes and staggers are given in Figs. 4 and 5. It will be seen that the three blade shapes were the C.4 profile of the National Gas Turbine Establishment based on circular-arc centre-lines of camber angle 20 deg, 30 deg and 40 deg respectively, the stagger angles were fixed at — 34 deg, — 36 deg and — 38 deg respectively, the blade chord was 6 in., the pitch/chord ratio unity and the aspect ratio 3. There were nine blades in each cascade, the three blades on each side of the middle three were cast in dental plaster. The surfaces of the blades were painted with several layers of Phenoglaze, smoothed with carborundum paper, which resulted in the blades having comparatively hard and smooth surfaces. The middle three blades were fabricated using brass bridge pieces of the correct aerofoil shape, the bridge pieces being attached to each other by brass rods placed in the direction of the blade length, excepting that the middle blade, on which the static-pressure readings were to be taken, had static-pressure tubes instead of rods. In the middle blade there were 44 tubes each leading to a 0·020-in. diameter static-pressure hole drilled on the central cross-section of this blade, where the pressure measurements were taken. In each of the middle three blades the space between the bridges was fared off by dental plaster, to the correct shape and finally the blades were painted similar to the other blades in the cascade. The blades were then mounted in the wooden frameworks of the cascades, each of which was 48 in. long resulting from 8-blade passages each of 6-in. pitch. At the cascade exit the side walls extended only about 1 in. beyond the blade trailing edges (*see* Fig. 3). The provision of longer side walls was not expected to affect the mid-span performance.

At that end of the cascade where the blade passage is convex, the boundary layer due to the tunnel wall would tend to cause separation of the air from the convex surface. This boundary layer was therefore sucked off through a $\frac{1}{2}$-in. wide slot, formed in the tunnel wall adjacent to the leading edge of this blade, extending over its full length. For this a separate fan operating as an exhauster was installed. The duty of this fan was to suck off an amount of air up to about 15 per cent of all the air which flowed through one blade passage. The air was sucked through the slot into a box mounted on the end of the cascade, which was connected to the exhauster by two 5-in. diameter pipes. The suction arrangements were designed so that the air would be sucked off approximately uniformly over the whole blade length.

3.2. *Wind Tunnel.*—The size of blades and cascades adopted, together with the range of Reynolds numbers to be covered, resulted in a desired rate of air flow of almost 50,000 cu ft per min. The design and development of this tunnel are described in Ref. 1. A sketch of the arrangement is given in Fig. 1, and photographs of the test assembly in Figs. 2 and 3.

The design was such that the cascades could be bolted on to the wooden ends of the tunnel. Making-up pieces of the correct taper were inserted to adjust the inlet air angle α_1 to the desired value. The internal width of the tunnel end was 18 in. to accommodate the blades lengthwise, but the internal height of the tunnel end had to be adjusted to suit each different value of α_1.

Arrangements were provided at the tunnel end so that traverses of the angle of flow, total head and static pressure could be made in the plane of the central cross-section over the middle three blades, at one chord distance upstream and one chord downstream of the cascade leading

and trailing edges respectively. On the inlet side of the cascade, a sliding shutter was fitted in the tunnel wall to prevent air leakage during the inlet traverses. The traversing gear, operated by a friction drive, was mounted on a graduated tube supported at the side of the tunnel. This can be seen in the photograph of Fig. 3. The traversing gear carried the tubes for measurement of total head, static pressure and angle of flow. The arrangement of these tubes was similar to that described by Harris and Fairthorne in Ref. 3. The zero angle of the yaw-meter was calibrated in a separate test by blowing air down a hollow tube, the angle of inclination of the hollow tube being measured by an accurate clinometer.

Due to the necessity for pressure plotting, which involves taking large numbers of static-pressure readings very quickly, it was decided to use a multi-tube tilting manometer of the National Physical Laboratory pattern having 36 tubes. This was suitable for measuring pressures accurately down to the small values resulting from air velocities at inlet to the cascades of about 30 ft/sec. For the lowest inlet air velocities, *i.e.*, from 30 ft/sec down to 10 ft/sec a Chattock gauge was used. This was sensitive to pressure heads of the order of 1/4,000 in. of water, which seemed to be satisfactory.

A traverse was taken over the rectangular area at inlet to one of the cascades to investigate any non-uniformity of total head, velocity and angle of flow. The traverse was made using the 30-deg camber cascade at an inlet air angle α_1 of 50 deg and at a Reynolds number of $2{\cdot}67 \times 10^5$. The results showed that, over the proposed test length, the variation of (*a*) total head in excess of atmospheric, and (*b*) velocity, did not exceed plus and minus $\frac{1}{2}$ per cent of the mean values, and the variation in inlet air angle did not exceed plus and minus 20 minutes. These variations were considered to be small enough for the programme of cascade tests.

The longitudinal component of the intensity of turbulence in the main stream at inlet to the cascade was measured by a hot-wire apparatus. Readings were taken at a point just upstream of the central cross-section of the middle blade of the cascade. Using a tunnel exit area which corresponded to an inlet air angle α_1 of 50 deg and over a range of air velocities from 40 to 100 ft/sec, the intensity of turbulence was found to be approximately $0{\cdot}22$ per cent. This was considered to be sufficiently small for this programme of cascade tests. It was intended that this programme should be followed by other tests, in which the main stream turbulence at inlet to the cascades was increased up to about 3 per cent, in order to observe the effect of increased turbulence on boundary-layer separation.

4. *Tests.*—4.1. *Programme of Cascade Tests.*—The three cascades were tested over a range of actual Reynolds numbers of 3×10^4 to 5×10^5, based on the inlet air velocity and on the blade chord. This resulted in the air velocity at inlet to the cascades ranging from 10 ft/sec to 160 ft/sec. Six groups of tests were carried out corresponding to nominal values of the inlet air angle α_1 of 35deg, 40 deg, 45 deg, 50 deg, 55 deg and 60 deg respectively. Measurements were taken of the distribution of the static pressure over the surface of the middle blade of each cascade at the central cross-section. Traverses were made of static pressure, total head and angle of flow at inlet and outlet from each cascade in the plane of the central cross-section, at one chord distance upstream of the leading edge and one chord downstream of the trailing edge respectively.

4.2. *Cascade Test Procedure.*—Since during any one test it was not practicable to take, at the same time, the inlet and outlet traverses and the static-pressure readings at the blade surfaces, careful procedure had to be adopted to ensure that all the pressure readings for any one test, related to the same air volume through the cascade. This was done by reading the static pressure in the tunnel, at a point where the air velocity was small, that is at the point A in Fig. 1. Since it was known that the pressure readings at the cascade would be closely proportional to the tunnel static pressure, the procedure was to run during any one test, at approximately the same tunnel static pressure. A small correction was applied to any of the readings which did not correspond exactly to the chosen tunnel static pressure for that test and therefore for the same volume flow during the test.

A typical graph of the inlet static pressure plotted against distance along the cascade is shown in Fig. 6. This was taken by pressure tappings in the side wall of the tunnel end, one chord distance upstream of the cascade leading edge. In every test the boundary-layer suction was adjusted until the inlet static-pressure distribution was uniform over as much as possible of the cascade length. The amount of air sucked off was kept at a constant rate during any one test, by noting the pressure drop across an orifice through which all the air was sucked and adjusting the rate of flow to maintain a constant pressure drop.

Initially the traversing at inlet and outlet to a cascade in the plane of the central cross-section extended over the middle three blades of each cascade. This was soon reduced to extend over two blades only, as it was felt that the additional labour resulting from the longer traverse was unnecessary.

At the beginning of the programme of testing, thirteen tests on each of the three cascades were carried out at each value of the inlet air angle α_1. These tests were approximately equally spaced over the full range of Reynolds number. Later in the programme some of the individual tests were omitted as these were thought to be unnecessary.

5. *Test Results.*—Figs. 7 and 8 show typical traverses of total head and angle of flow at one chord distance downstream of the trailing edge in the plane of the central cross-section. These are for the lowest and highest Reynolds number tests carried out at a medium value of the inlet air angle α_1.

The effect of Reynolds number on the inlet and outlet air angles is shown by Figs. 9 to 17, on the contraction at outlet by Figs. 18 to 20 and on the loss of head through the cascades by Figs. 21 to 26.

Figs. 27 to 44 show the plots of static pressure over the surface of the middle blade of each cascade at the central cross-section. The pressures are plotted on a non-dimensional basis, the ordinate being the static pressure at the point on the blade surface minus the static pressure at outlet from the cascade, expressed as a fraction of the outlet velocity head. This is in line with the recommendation of Howell and Carter in Ref. 2. This basis of pressure plotting facilitates comparison with turbine cascades and with isolated aerofoils, since the values of static pressure near the trailing edge are numerically zero for all these arrangements.

Figs. 45 to 47 show the blading efficiency plotted against the actual Reynolds number. This efficiency has been calculated from:

$$\text{Efficiency} = 1 - \frac{\text{total-head loss}}{\text{reduction of velocity head}}.$$

In the calculations of efficiency, the readings were weighted for mass flow before integrating the losses. This is the so-called energy method which evaluates the energy in the air at the inlet and outlet traverses. Due to the gradual dissipation of the blade wakes in the air flowing from the cascade, the value of this efficiency will be dependent to some extent on the position of the outlet traverse. Assuming that the air velocity ultimately becomes uniform in a two-dimensional manner, the principle of constant momentum can be applied to the air stream between the outlet traverse plane and the plane where uniformity has occurred, and the small loss of energy during this smoothing out process can be evaluated. The so-called momentum method of evaluating the efficiency includes this small loss of energy with the loss in the cascade giving an efficiency which is therefore independent of the position of the outlet traverse, and whose value is slightly lower than that plotted in Figs. 45 to 47. It can be shown (*see* Ref. 4) that the evaluated efficiencies by the momentum method are approximately the same as those obtained by not weighting the energy readings for mass flow before integrating the losses at the actual traverse positions.

6. *Discussion of Results.*—6.1. *Three-dimensional Effects.*—In these tests, since the boundary layers at the tunnel side walls were not sucked away, there was a gradient of inlet velocity over the end portions of the blades where they project into the boundary layers. This resulted in

secondary flows which induced a modified flow at the cascade exit. The programme of tests has been mainly concerned with traverses in the plane of the blade central cross-sections one chord distance upstream and downstream of the blades, so that the induced effects at this outlet traverse position should be considered. Since the tunnel boundary-layer thickness was small in comparison with the blade length, it would appear, therefore, that the induced secondary effects on the centre-line were relatively small. The effect on the mean loss of total head was negligible. The question of secondary flow and the resulting effects in these cascades are discussed in Ref. No. 5.

One of the important factors in modifying the numerical values of the results is the lateral contraction of the air stream in the cascade and at exit from it. A measure of this contraction is given by the so-called percentage contraction, calculated from the readings taken in the plane of the blade central cross-sections, one chord distance upstream and downstream of the blades. This percentage contraction is given by :

$$\left(1 - \frac{V_1 \cos \alpha_1}{V_2 \cos \alpha_2}\right) \times 100 \text{ per cent},$$

in which V is the air velocity and the suffixes 1 and 2 refer to the inlet and outlet traverses respectively. Values are plotted in Figs. 18 to 20. It will be seen that large values of this contraction are associated with large air deflections, but that the contraction is not greater than about 10 per cent until deflections exceed 20 deg. This contraction produces an acceleration in opposition to the diffusing effect of the cascades, which results in the static-pressure rise being less than that calculated from the measured deflections, assuming two-dimensional flow. Also the static-pressure distributions over the surface of the middle blade at the central cross-section do not correspond to two-dimensional flow. Adverse pressure gradients are reduced and boundary-layer separation from the blade surfaces tends to be suppressed. Therefore it is necessary in the interpretation of test results giving pressure distributions, efficiency and air deflection, to evaluate and specify the contraction, associated with particular test results.

A description is given in Ref. 4 of results obtained in an electric tank to give the two-dimensional potential-flow solution of static-pressure distribution. A set of model blades was used of identical shape and setting to the 40-deg camber blades as used in the wind-tunnel tests. These model blades were tested under conditions which corresponded to the same range of inlet angle as in the wind-tunnel tests. An empirical method was developed for correcting the two-dimensional potential-flow pressure distributions, as given by the electric tank, to give distributions having the same contraction through the cascade, as occurred in the wind-tunnel tests. The cases considered were at the highest inlet Reynolds numbers, because for these cases the boundary-layer thicknesses on the blade surfaces were small and therefore caused only slight modification to the potential-flow distributions.

6.2. *Boundary-layer Separation.*—Separation from the blade surfaces increases the losses seriously reducing the efficiency of the cascades, as can be seen in Figs. 45 to 47. The effect of separation can be detected on the curves of static-pressure distribution over the blade surfaces, as a reduction in the positive pressure gradient (*see* Figs. 27 to 44). When separation is complete the curves are horizontal with no further rise of static pressure. An example of this can be seen in Fig. 36, which shows the effect of laminar separation at low Reynolds number on the convex surface of the blades of the 30-deg camber cascade at an incidence of — 1 deg. Separation results in the pressure at the trailing edge being less than the outlet static pressure, so that when the pressure-distribution curves are extrapolated to the trailing edge the ordinates there are negative.

When transition occurs in the boundary layer before the laminar separation point is reached, separation of the laminar layer does not occur and the local pressure rise is maintained after transition. This procedure tends to occur at the higher inlet Reynolds numbers, and can also be

seen on the convex surface of the blades in Fig. 36. On reducing the inlet Reynolds number the point of transition moves back towards the trailing edge, whereas the point at which laminar separation is likely to occur remains approximately fixed until the Reynolds number is reduced to a very low value. This is pointed out in section 6.3. Hence the point of transition moves back until it reaches the separation point. Further slight reduction of the inlet Reynolds number, therefore, causes separation to commence. This is discontinued at transition when the boundary layer returns to the surface in the turbulent form. Further reduction allows separation to develop fully before transition and there is then no further rise of static pressure. This process can be observed in Fig. 36, partial separation showing as a hump on the pressure-distribution curves, and is the so-called ' bubble of turbulence ' referred to in Ref. 6. It will be seen from these curves that the hump grows larger as the Reynolds number is decreased until separation is complete.

Separation affects the outlet traverses of total head by broadening the wakes to the extent, in some cases, of covering the full pitch of the blades. An example of this can be seen by comparing Figs. 7 and 8.

Separation reduces the air deflection by increasing the outlet air angle α_2. This reduces the efficiency still further. An example of this increase of outlet air angle can be seen by comparing the traverses in Figs. 7 and 8. The angle is fairly uniform between the wakes. The variation within the wakes is fictitious and due to the inability of the claw-type yawmeter to read the angle correctly, when placed in a region having a transverse gradient of total head.

In these tests the following types of separation occurred :

(i) From the convex surfaces of the blades :

(a) Complete laminar separation at low Reynolds numbers, occurring in the following cases :

Cascade camber (deg) ..	20			30					40					
α_1 (deg)	35	40	45	35	40	45	50	55	35	40	45	50	55	60
Angle of incidence (deg) ..	−9	−4	+1	−16	−11	−6	−1	+4	−23	−18	−13	−8	−3	+2
Fig. No.	27	28	29	33	34	35	36	37	39	40	41	42	43	44

It will be noticed that reducing the incidence increases the tendency to this type of separation.

(b) Partial laminar separation at rather higher Reynolds numbers, occurring in the following cases :

Cascade camber (deg)	20				30						40				
α_1 (deg)	35	40	45	50	35	40	45	50	55	60	40	45	50	55	60
Angle of incidence (deg)	−9	−4	+1	+6	−16	−11	−6	−1	+4	+9	−18	−13	−8	−3	+2
Fig. No.	27	28	29	30	33	34	35	36	37	38	40	41	42	43	44

It will be noticed that with the 40-deg camber cascade at an angle of incidence of − 23 deg (Fig. 39) laminar separation from the convex surface was complete over the full range of Reynolds number.

(c) Partial laminar separation near the leading edge at high positive incidences, occurring in the case of the 20-deg camber cascade at an angle of incidence of 16 deg (Fig. 32).

This separation seems to be followed quickly by transition, after which there is considerable pressure recovery but with reattachment of the turbulent layer apparently incomplete, resulting in a very low efficiency, as can be seen in Fig. 45.

(*d*) Turbulent separation at high Reynolds numbers, occurring in the case of the 20-deg camber cascade at an angle of incidence of 11 deg (Fig. 31) and the 30-deg camber cascade at an angle of incidence of 9 deg (Fig. 38).

(*e*) Separation at low Reynolds numbers near the trailing edge, in the 30-deg camber cascade at an angle of incidence of 9 deg (Fig. 38). This is likely to be turbulent separation occurring due to the large increase in boundary-layer thickness at low Reynolds numbers.

(ii) From the concave surfaces of the blades:

These separations are mainly near the leading edge, where the surfaces are actually convex.

(*a*) Laminar separation occurring near the leading edge at the higher Reynolds numbers in the case of the 40-deg camber cascade at the high negative incidence of — 23 deg (Fig. 39). This disappears at lower Reynolds numbers.

(*b*) Partial laminar separation occurring in the following cases:

Cascade camber (deg)	30			40				
α_1 (deg)	35	40	45	35	40	45	50	55
Angle of incidence (deg)	—16	—11	—6	—23	—18	—13	—8	—3
Fig. No.	33	34	35	39	40	41	42	43

It will be noticed that in this type of separation also, reducing the incidence increases the tendency to separate.

6.3. *The Laminar Layer.*—In Ref. 7 Thwaites has developed equations predicting the growth and separation of the laminar boundary layer. This method, developed from the von Kármán momentum equation, results in a non-dimensional form parameter for the velocity distribution across the laminar layer, which is a function both of the velocity in the main stream just outside the boundary layer and the distance from the leading edge. This parameter is shown to be proportional to the velocity gradient along the blade surface just outside the boundary layer. Separation is expected to occur when this parameter reaches a given value. According to this method, therefore, the position of the laminar-separation point is determined by the form of the non-dimensional pressure distribution over the blade surface up to that point. Since this distribution remains constant over a wide range of inlet Reynolds number the position of laminar separation is approximately independent of variations in the inlet Reynolds number. In the cascade tests, it was found that when the Reynolds number was reduced to very low values the laminar-separation point was somewhat delayed. This can be explained by Thwaites' analysis, which indicates that for similar pressure distributions the momentum thickness is inversely proportional to the square root of the inlet Reynolds number. Hence as the Reynolds number is reduced to a low value the displacement thickness increases to a large value. This results in an effect on the pressure distribution which is somewhat similar to that caused by the lateral contraction of the air stream, in that it reduces the positive pressure gradients. This has the effect of delaying laminar separation.

The relative positions of laminar separation and transition are of great importance in deciding the performance of the blades. In these tests important factors affecting transition are Reynolds number and pressure gradients on the blade surface. As already pointed out reducing the

Reynolds number delays transition. Negative pressure gradients also delay transition and cause it to be more gradual when it does occur. On the other hand large positive pressure gradients tend to promote it.

In Ref. 4 Stuart has applied Thwaites' equations to the cascade tests. He considered the three cascades at various values of the inlet air angle α_1 and Reynolds numbers of approximately 2×10^5 and 5×10^5. The positions of laminar separation predicted by this method agree well with the experimental results.

Experiments have also been carried out to study the boundary-layer behaviour by observing a smoke filament introduced into the main air stream through a narrow slot in the suction surface of one of the blades near the leading edge. These tests showed the following three types of flow as the Reynolds number was reduced: (*a*) smooth uninterrupted flow with the turbulent layer adjacent to the surface, (*b*) local separation of the laminar layer enclosing a ' bubble of turbulence ', followed by the turbulent layer adjacent to the surface, and (*c*) complete laminar-layer separation. These tests therefore gave the position of separation, which was found to agree with the cascade results and with the theoretical predictions using Thwaites' equations.

At high positive incidences there seems to be a critical incidence above which efficiencies fall rapidly. See for example Fig. 45, for the 20-deg camber blade at an inlet air angle α_1 of 60 deg (incidence + 16 deg). The corresponding pressure distributions in Fig. 32 show a very sharp suction peak close to the leading edge on the convex surface of the blades, followed by a steep positive pressure gradient. The theoretical considerations based on Thwaites' equations confirm that separation will occur with such a pressure distribution soon after the suction peak, even although this is close to the leading edge, providing the positive pressure gradient is very steep. On a moderate reduction of the incidence from this very high positive value, the suction peak becomes less sharp and the positive pressure gradient less steep. This is a type of pressure distribution which tends to give good performance, because the positive pressure gradient is not steep enough to produce early separation, but is however steep enough to give appreciable pressure rise after the suction peak. This is beneficial in promoting early transition before separation tends to occur. If the suction peak is smaller still, rounder and occurs further from the leading edge, separation will tend to occur in smaller positive pressure gradients because of the greater distance from the leading edge, whilst the pressure rise subsequent to the suction peak is so small that transition is delayed.

6.4. *The Turbulent Layer.*—Usually there is a considerable pressure rise occurring in the turbulent layer on the convex surface of the blades, so that it is of importance to consider the behaviour of the turbulent layer in a positive pressure gradient. Fortunately, the turbulent layer is able to remain in contact with the blade surface even in the presence of considerable increases of static pressure. However, there were some cases of turbulent boundary-layer separation observed in the tests, as is illustrated in the case of the 30-deg camber cascade at an α_1 of 60 deg, as seen in Fig. 38. This takes the form of a flattening of the pressure-distribution curve near the trailing edge at the highest Reynolds number. This results in the efficiency curve beginning to fall at the higher Reynolds numbers, as is seen in Fig. 46. Hewson in Ref. 8 has developed equations to determine the point of turbulent boundary-layer separation. Stuart in Ref. 4 has applied these equations to the cascade results. In the few cases where there is turbulent separation, Hewson's equations locate the positions of separation at points agreeing with the cascade results.

Since the skin friction per unit area in the turbulent layer is greater than in the laminar layer it would be expected that as the Reynolds number is increased, resulting in earlier transition, the skin-friction coefficient for the blades would also increase, and the advantage of designing for early transition to avoid laminar separation at low Reynolds numbers would be partly offset by the increased skin-friction drag at high Reynolds numbers. However, the loss of total head curves in Figs. 24 to 26 show that, providing turbulent separation has not occurred, there is no appreciable increase of total-drag coefficient on increasing the Reynolds number. This means that the increase in skin-friction coefficient is approximately balanced by the reduction in the form-drag coefficient.

6.5. *Theoretical Velocity Distributions.*—In Ref. 4 theoretical velocity distributions over the blade surfaces have been derived, aimed at obtaining the maximum pressure rise without separation occurring. The criteria for separation devised by Thwaites in the laminar layer and Hewson in the turbulent layer have been used, together with assumed positions of the suction peak.

6.6. *Air Angles and Deflection.*—Curves of α_1 against α_2 at various Reynolds numbers are plotted in Figs. 15 to 17. It can be seen from these curves that when there was negative incidence, a reduction of Reynolds number caused large increases in α_2, due to the onset of laminar separation. The effect of Reynolds number on α_2 was small at positive incidences of 2 deg to 6 deg, and above about 6 deg increasing the Reynolds number caused increases in α_2, due to the onset of turbulent separation.

6.7. *Loss of Total Head.*—In Figs. 21 to 23 is plotted, for constant incidences, the log of the percentage loss of total head against the log of the Reynolds number. If tests at high positive and negative incidences are omitted, the results indicate that, at a constant incidence, there is an approximate straight-line relationship between these two co-ordinates. Therefore the percentage loss (L) is related to the Reynolds number (R) by an equation of the form $L = aR^n$, in which, for any one incidence, a and n are constants. The plotted results suggest the following approximate values for n:

Camber	..	20 deg	30 deg	40 deg
n	.. ..	−0·44	−0·56	−0·90

There was no general tendency for n to increase in the laminar separation region.

7. *Conclusions.*—At normal values of angle of incidence, there is an optimum Reynolds number for high efficiency. At extreme values of Reynolds number, separation of the boundary layer occurs from the convex surface of the blades: laminar separation at low values and turbulent separation at high values.

In the case of laminar separation the larger camber blades are worse, since on reducing the Reynolds number laminar separation occurs at a higher Reynolds number the larger the camber. The effect of this can be seen on the efficiency curves in Figs. 45 to 47. Freedom from laminar separation at rather low Reynolds numbers seems to result from a fairly sharp suction peak on the pressure distribution near the leading edge of the convex surface. This tends for transition to occur before laminar separation is able to develop, by delaying the tendency to separate and hastening transition to some extent. If the suction peak is too sharp it is likely that the very steep positive pressure gradient immediately after the suction peak will result in laminar separation. In addition in order to offset the chance of turbulent separation subsequently occurring, as the trailing edge is approached, the pressure rise from the suction peak to the trailing edge must not be excessive. A large pressure rise on the convex surface of the blades can be best attained if there is a fairly steep pressure gradient immediately after the suction peak, with the suction peak located close to the leading edge. This allows more of the pressure rise to occur in the laminar layer. The pressure gradient can then be progressively reduced in the turbulent layer as the trailing edge is approached. These desirable features are illustrated by the good performance, over a wide range of Reynolds number, of the 20-deg camber cascade at an air inlet angle α_1 of 50 deg. This can be seen in Figs. 30 and 45.

Promoting early transition in order to offset the tendency for the laminar layer to separate at low Reynolds numbers has the disadvantage that the skin-friction loss in the turbulent layer is increased. Appreciable reduction of skin-friction loss appears possible only in cases where performance at low Reynolds numbers is unimportant, in which case the transition point need not occur near the leading edge.

8. *Acknowledgments.*—This investigation was carried out in the Cambridge University Engineering Department, under the sponsorship of the Chief Scientist, Ministry of Supply, to whom acknowledgment is made for permission to publish this report.

Thanks are due to Mr. E. C. Deverson, of the Cambridge University Engineering Department, who has helped with the laborious work of taking and recording the readings in this programme of research.

REFERENCES

No.	*Author*	*Title, etc.*
1	H. G. Rhoden	The development of a wind tunnel. *Engineering*, Vol. 171, p. 677. June, 1951.
2	A. R. Howell and A. D. S. Carter	Fluid flow through cascades of aerofoils. *Proc. 6th Int. Congr. App. Mech.* 1946.
3	R. G. Harris and R. A. Fairthorne	Wind-tunnel experiments with infinite cascades of aerofoils. R. & M. 1206. September, 1928.
4	D. J. K. Stuart	Analysis of Reynolds number effects in fluid flow through two-dimensional cascades. R. & M. 2920. July, 1952.
5	W. D. Armstrong	An investigation of secondary flow in cascades of axial-flow compressor blades. A.R.C. 15,250. May, 1952.
6	G. B. McCullough and D. E. Gault	Examples of airfoil-section stall at low speed. N.A.C.A. Tech. Note 2502. September, 1951.
7	B. Thwaites	Approximate calculation of the laminar boundary layer. *Aero. Quart.*, Vol. 1. November, 1949.
8	C. T. Hewson	The growth and separation of a turbulent boundary layer. Ph.D. Thesis, Cambridge University. 1949.

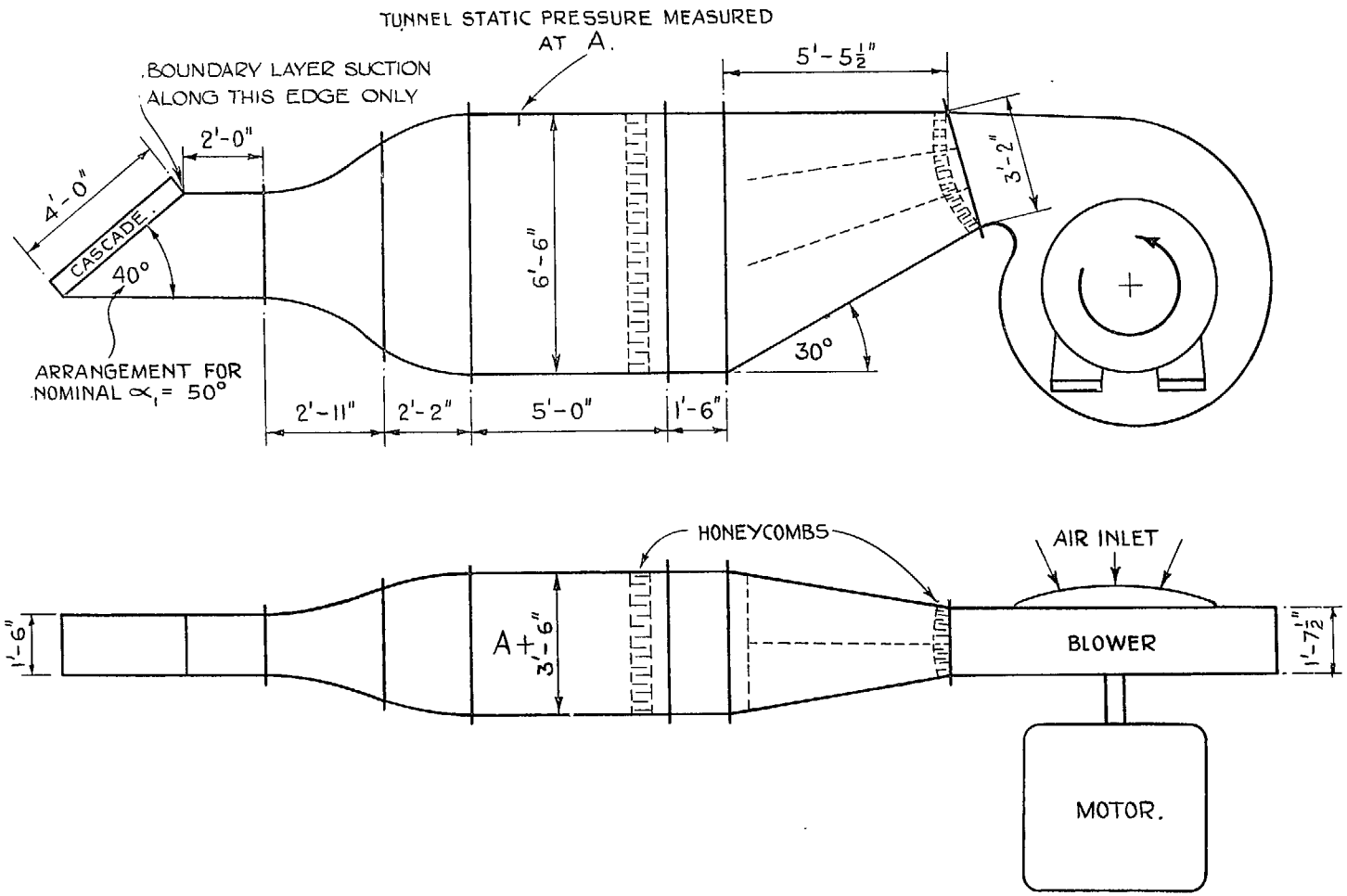

FIG. 1. Arrangement of tunnel.

FIG. 2. Wind tunnel.

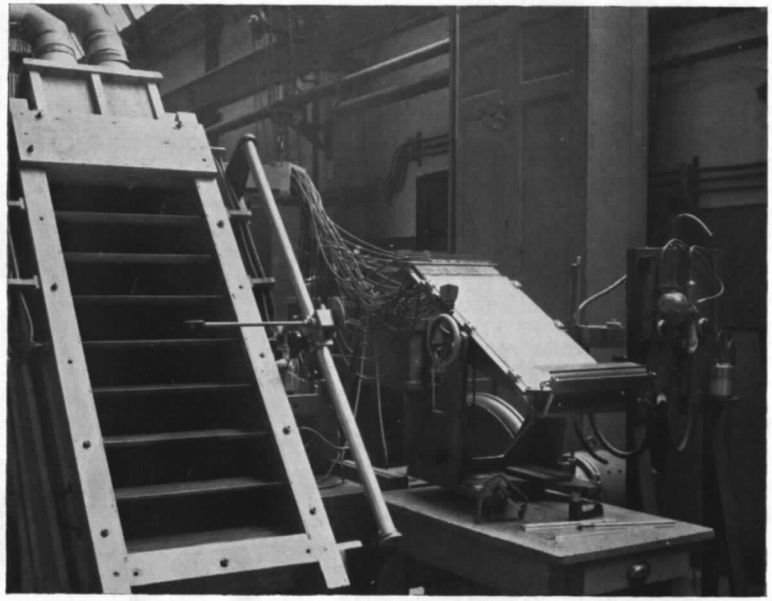

FIG. 3. Apparatus at tunnel exit.

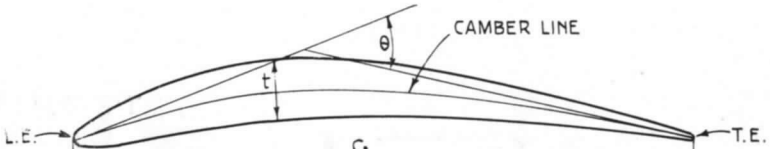

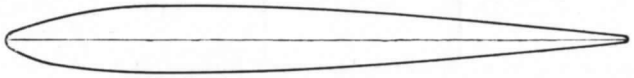

BASE AEROFOIL C4.

L.E. RAD = 12% t t/C = 10% T.E. RAD. = 6 % t

STATION.	0	1·25	2·50	5·00	7·50	10·0	15·0	20·0	30·0	40·0	50·0	60·0	70·0	80·0	90·0	95·0	100	} % OF C
UPPER & LOWER	0	1·65	2·27	3·08	3·62	4·02	4·55	4·83	5·00	4·89	4·57	4·05	3·37	2·54	1·60	1·06	0	

STATION OF MAX. THICKNESS = 30% C

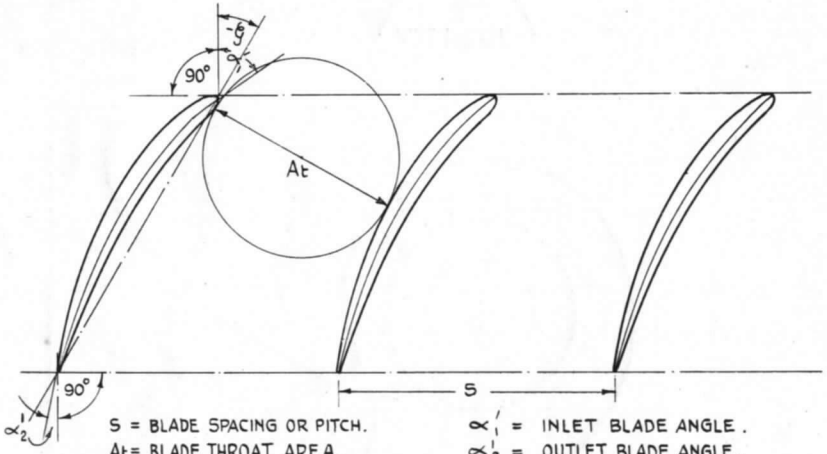

S = BLADE SPACING OR PITCH. α'_1 = INLET BLADE ANGLE.
At = BLADE THROAT AREA. α'_2 = OUTLET BLADE ANGLE.
ϑ = STAGGER ANGLE. ANGLE OF INCIDENCE = (INLET AIR ANGLE) − α'_1.

DIMENSIONS OF BLADES AND CASCADES TESTED.

BLADES 6 IN. CHORD, 18 IN. LONG. 9 BLADES IN CASCADE AT 6 IN. PITCH.
C.4. PROFILE ON CIRCULAR ARC CAMBERS. STAGGERS CHOSEN AS FOLLOWS TO GIVE APPROXIMATELY THE SAME OUTLET AIR ANGLE IN EACH CASE:

CAMBER ANGLE θ.	STAGGER ANGLE ϑ.	INLET BLADE ANGLE α'_1.	OUTLET BLADE ANGLE α'_2
20°	− 34°	44°	24°
30°	− 36°	51°	21°
40°	− 38°	58°	18°

FIG. 4. Compressor blade data.

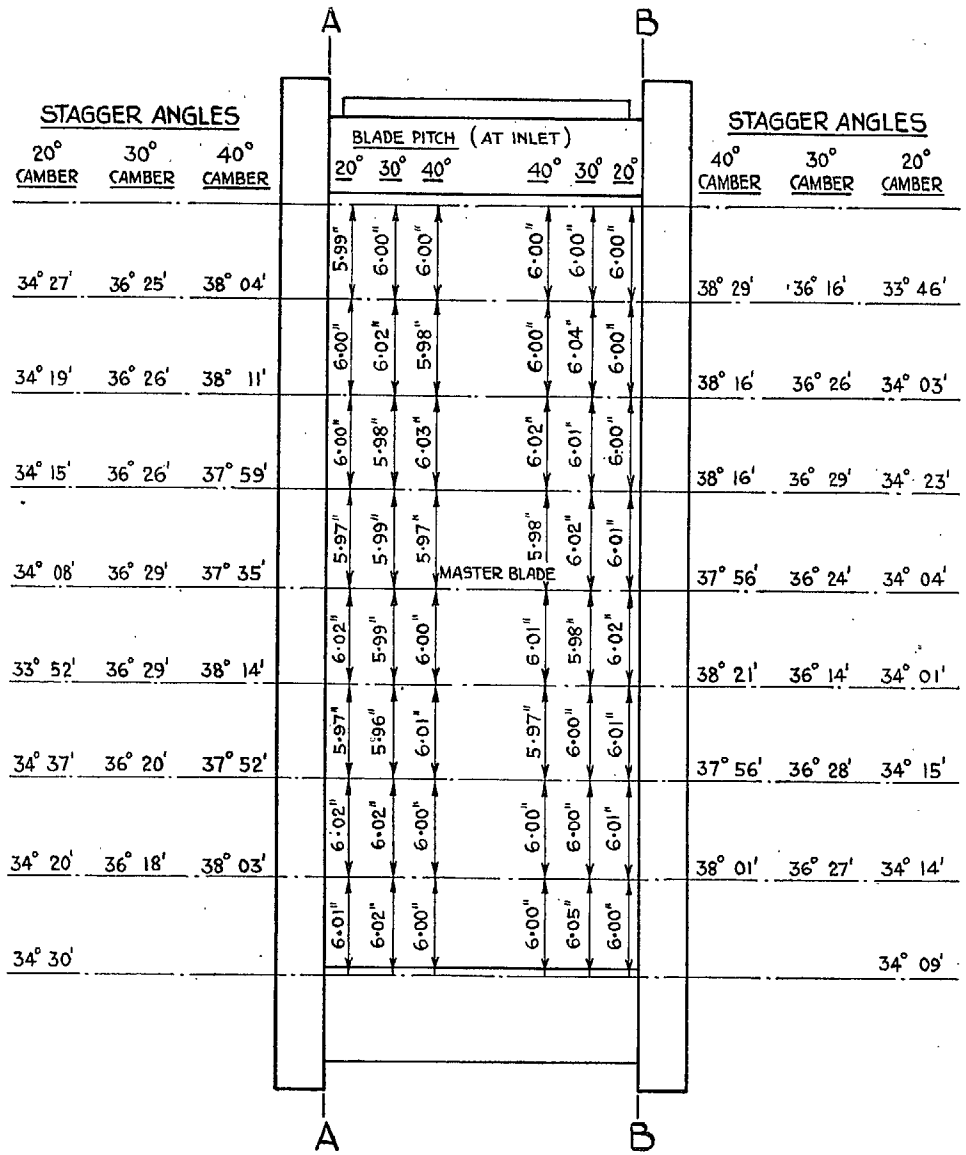

FIG. 5. View of cascade exit face. Actual blade pitch and stagger angles of 20, 30 and 40-deg cascades as manufactured, measured in the planes AA and BB.

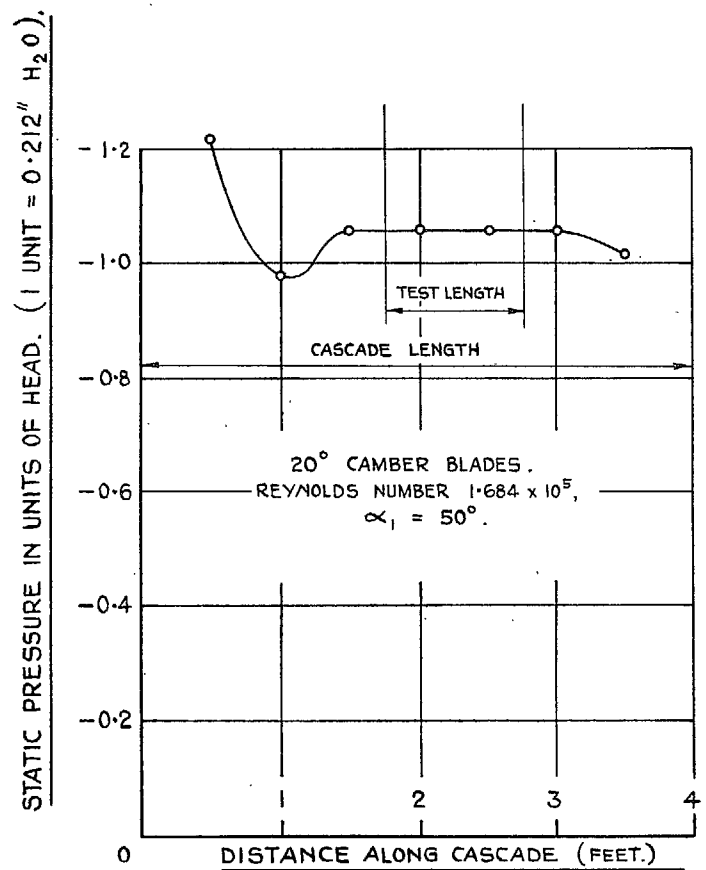

FIG. 6. Static pressure at cascade inlet. Typical distribution of pressure over cascade length, measured at tunnel wall, one chord upstream.

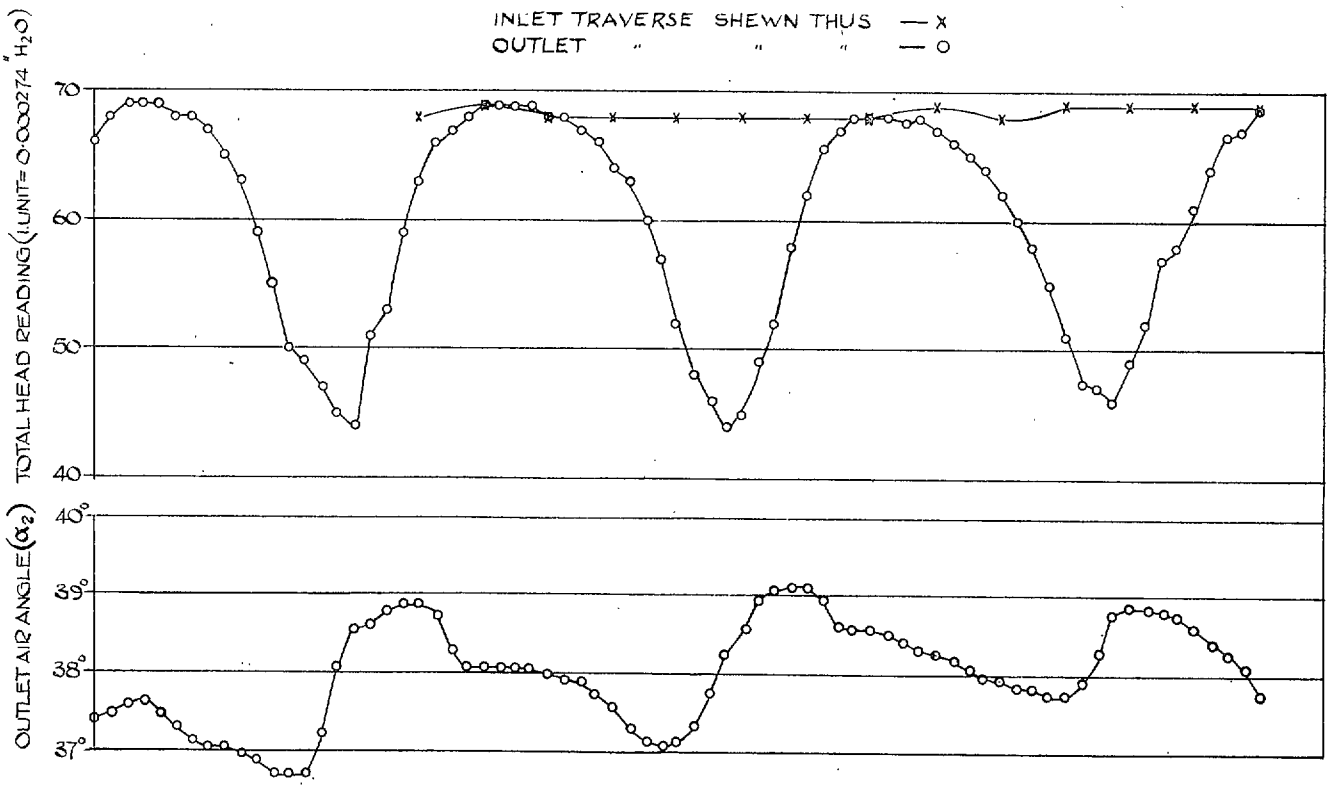

FIG. 7. Outlet traverses. 30-deg camber blades. Reynolds number = $0{\cdot}317 \times 10^5$. Nominal air inlet angle (α_1) = 50 deg.

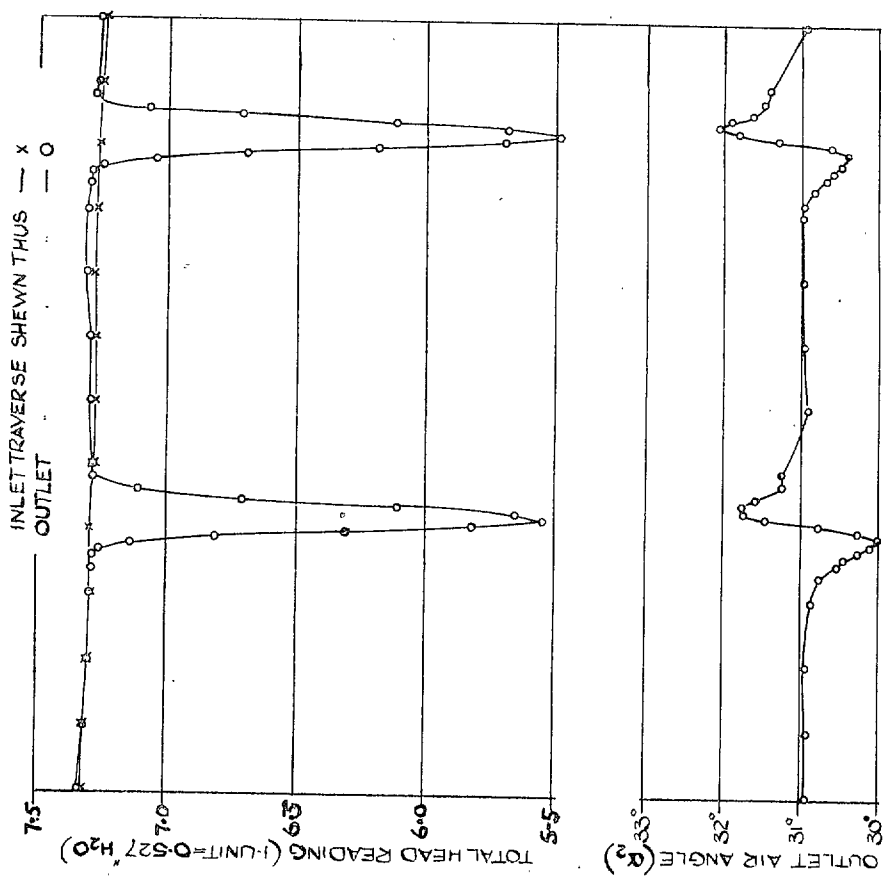

FIG. 8. Outlet traverses. 30-deg camber blades.
Reynolds number = $4{\cdot}78 \times 10^5$.
Nominal air inlet angle (α_1) = 50 deg.

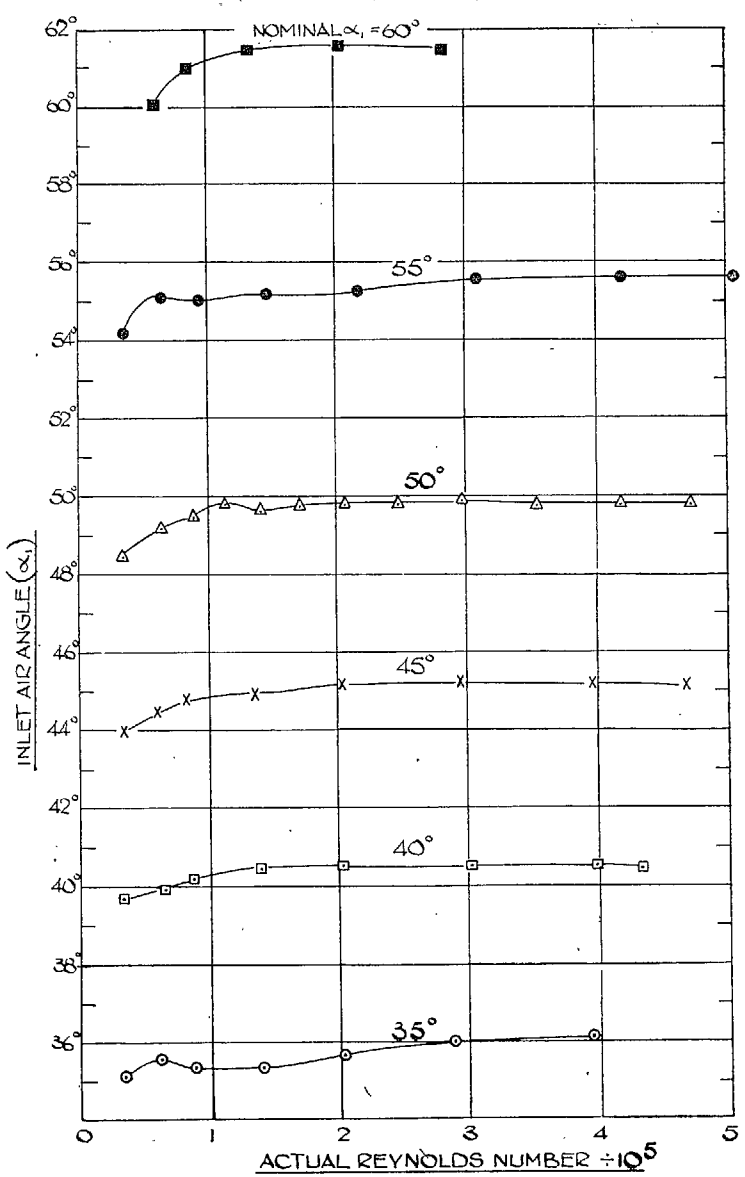

FIG. 9. Effect of Reynolds number on inlet air angle. 20-deg camber cascade.

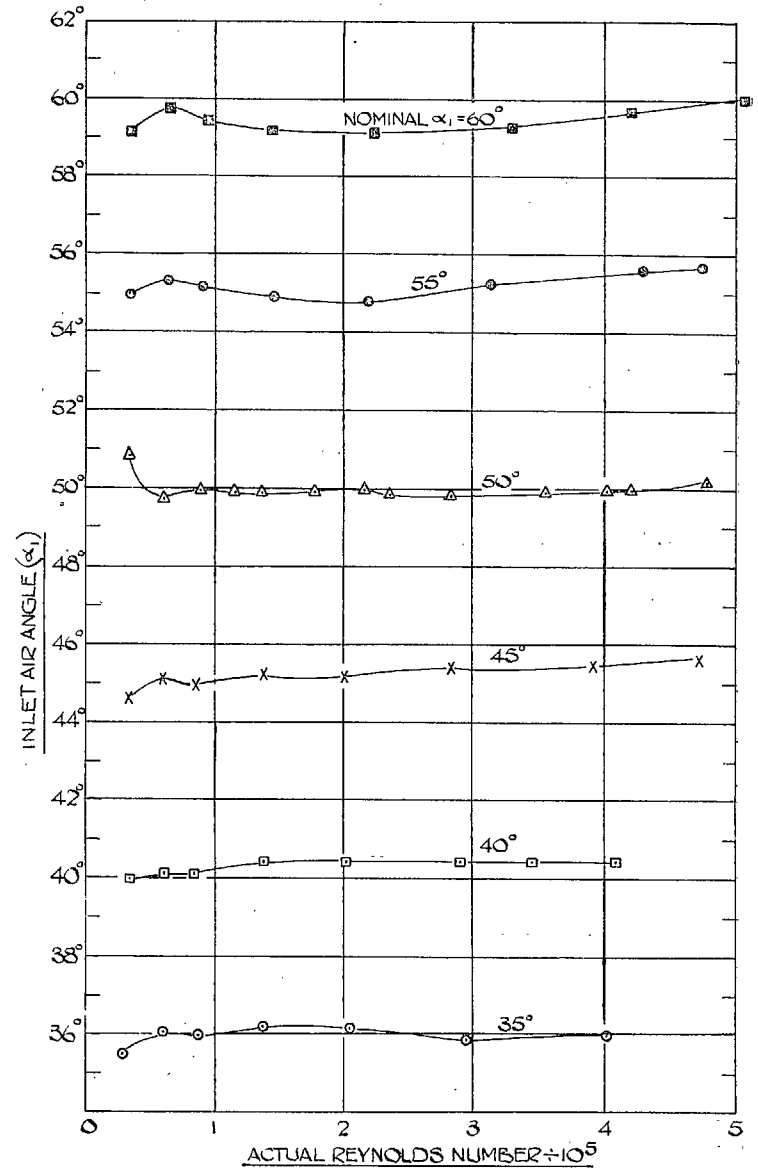

FIG. 10. Effect of Reynolds number on inlet air angle. 30-deg camber cascade.

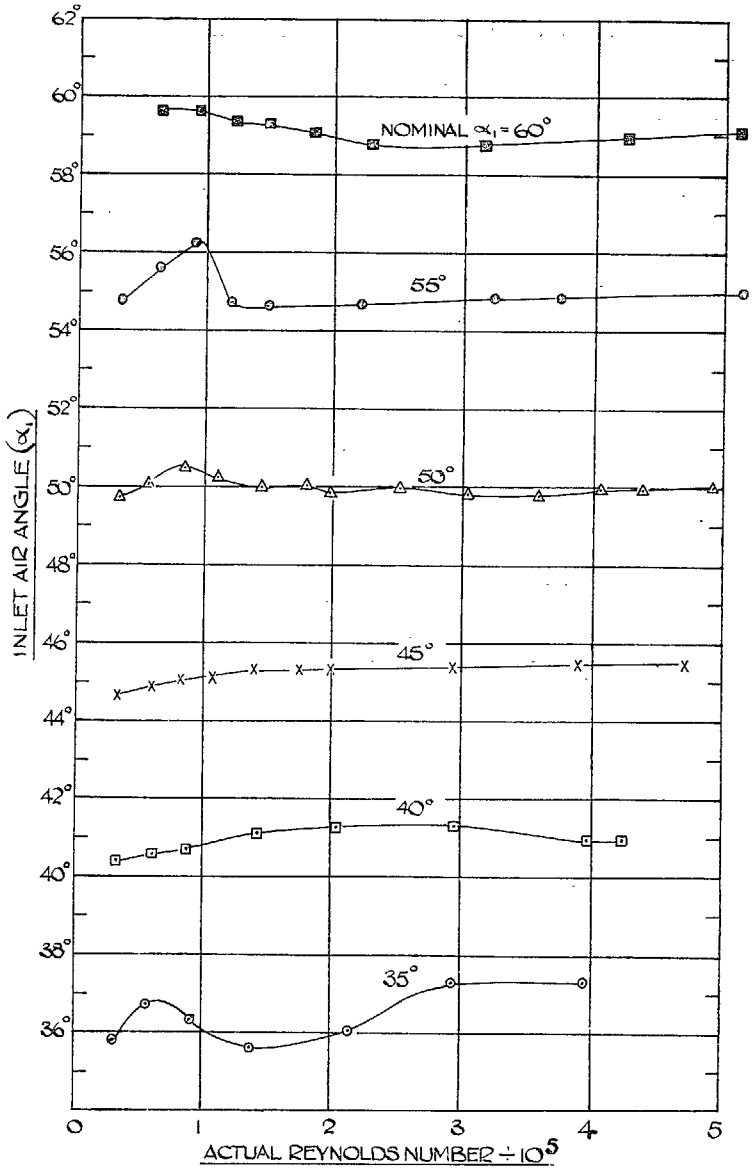

FIG. 11. Effect of Reynolds number on inlet air angle. 40-deg camber cascade.

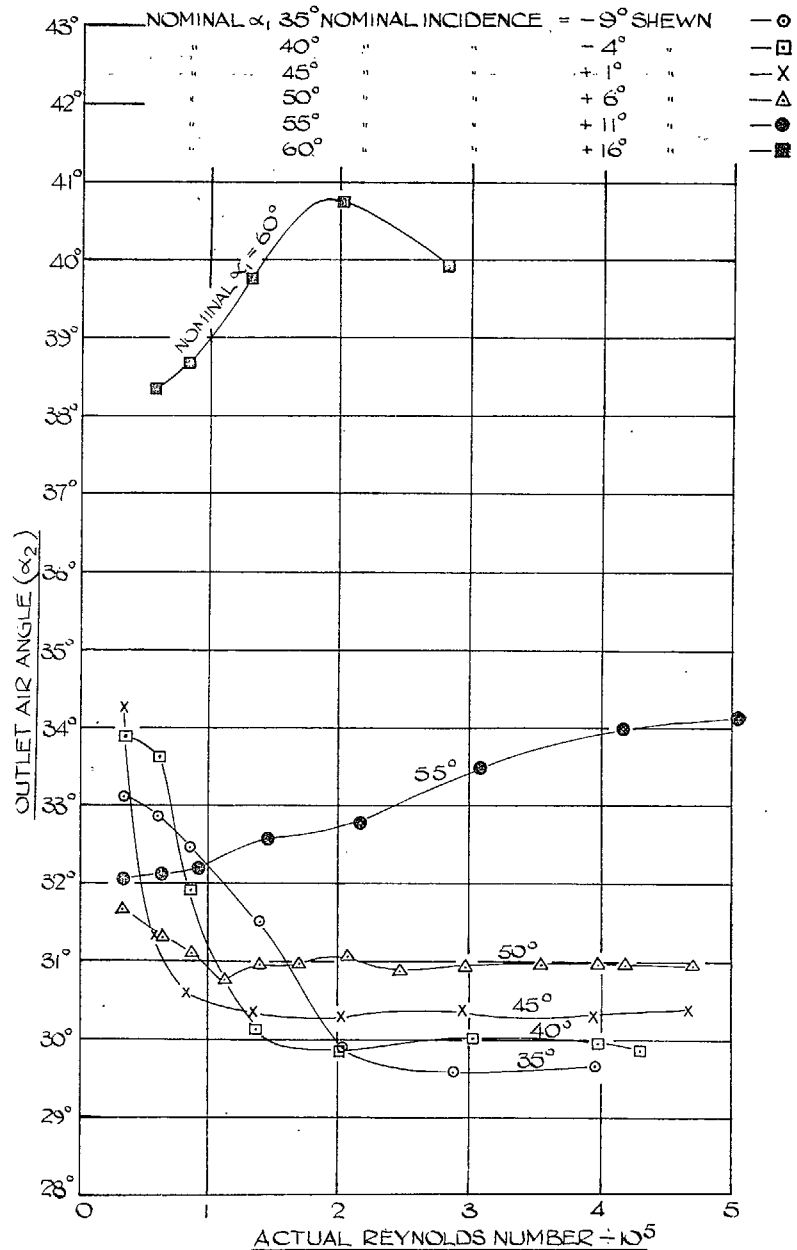

FIG. 12. Effect of Reynolds number and inlet air angle on outlet air angle. 20-deg camber cascade.

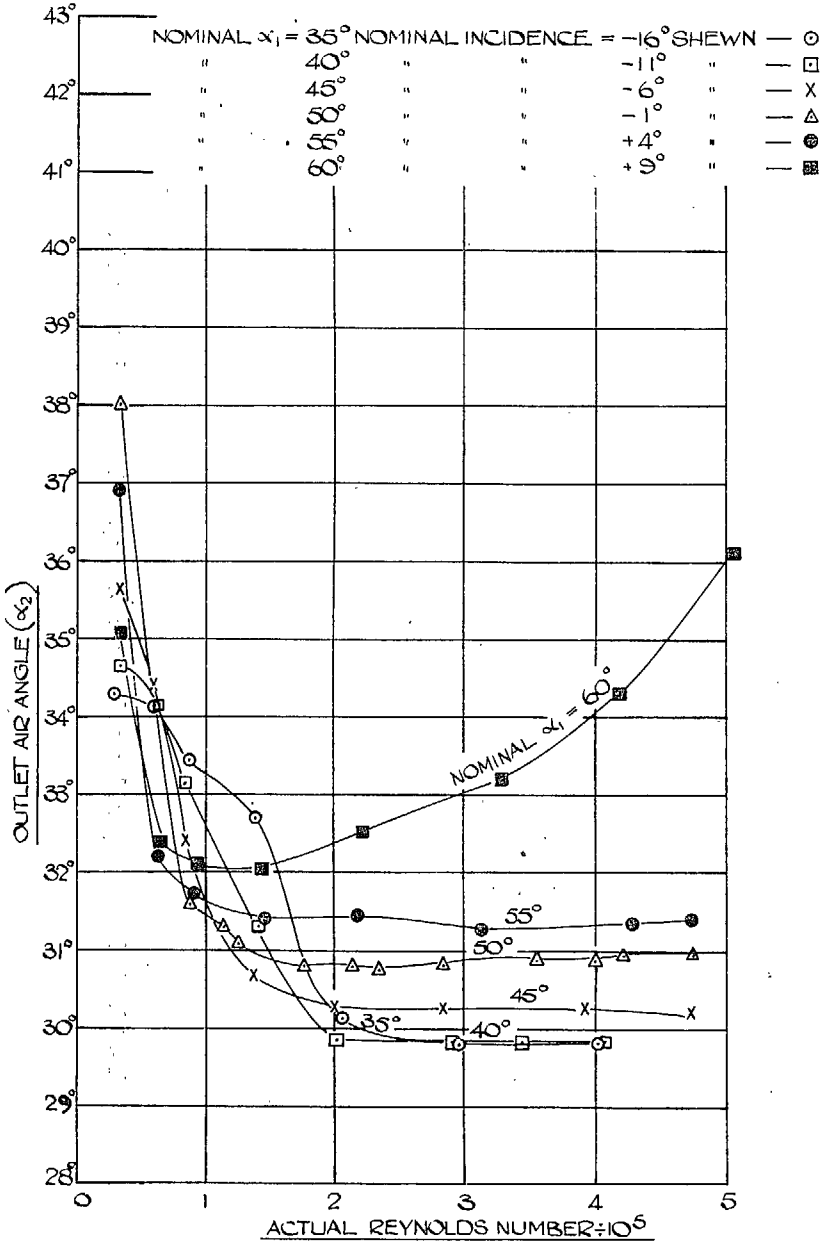

FIG. 13. Effect of Reynolds number and inlet air angle on outlet air angle. 30-deg camber cascade.

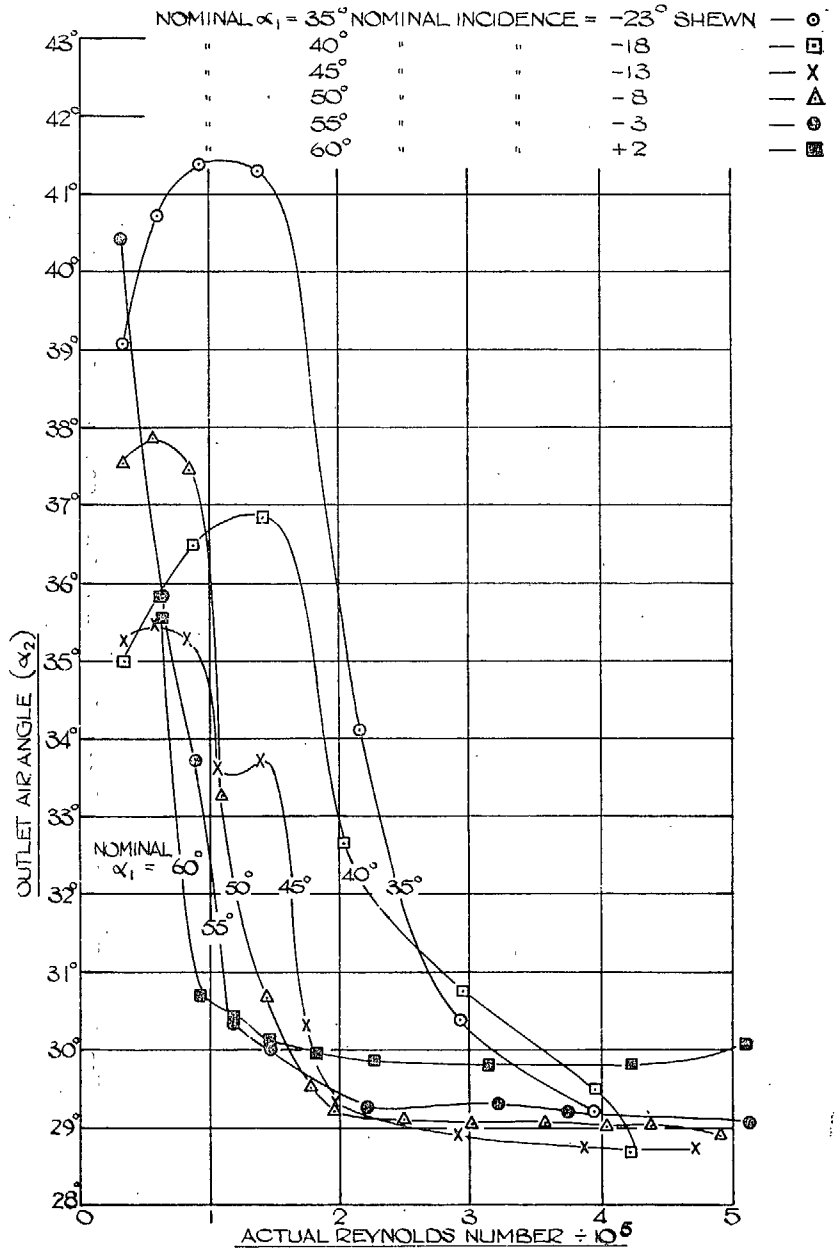

FIG. 14. Effect of Reynolds number and inlet air angle on outlet air angle. 40-deg camber cascade.

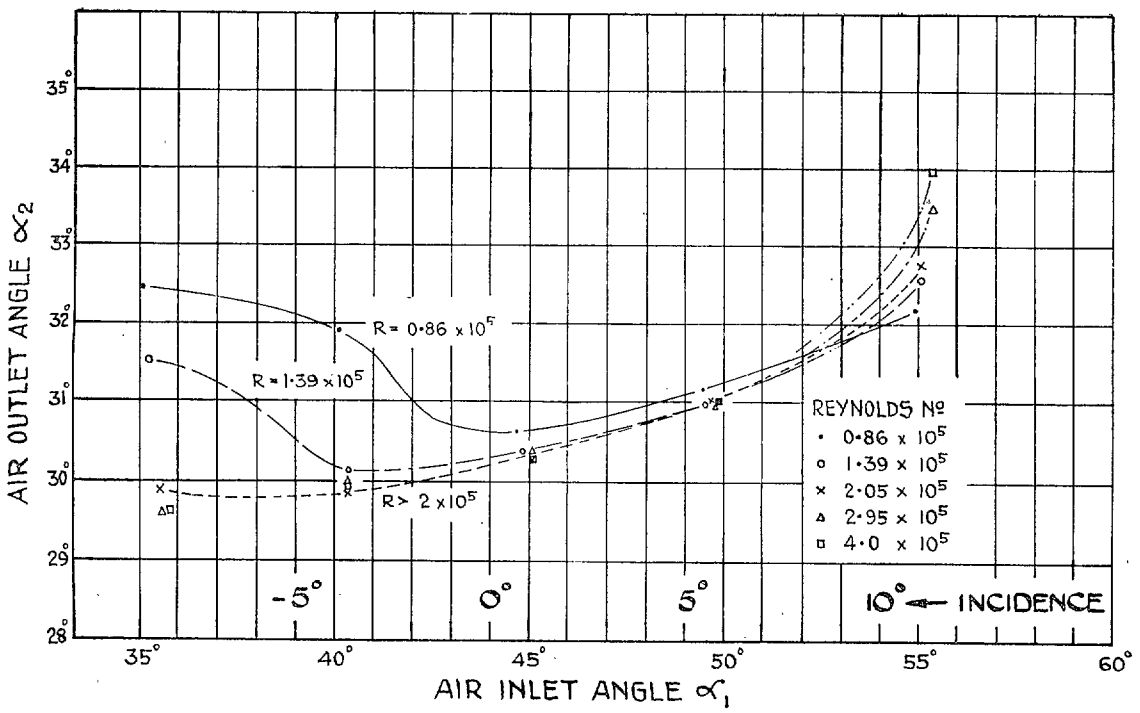

FIG. 15. Effect of Reynolds number on α_1 and α_2. 20-deg camber cascade.

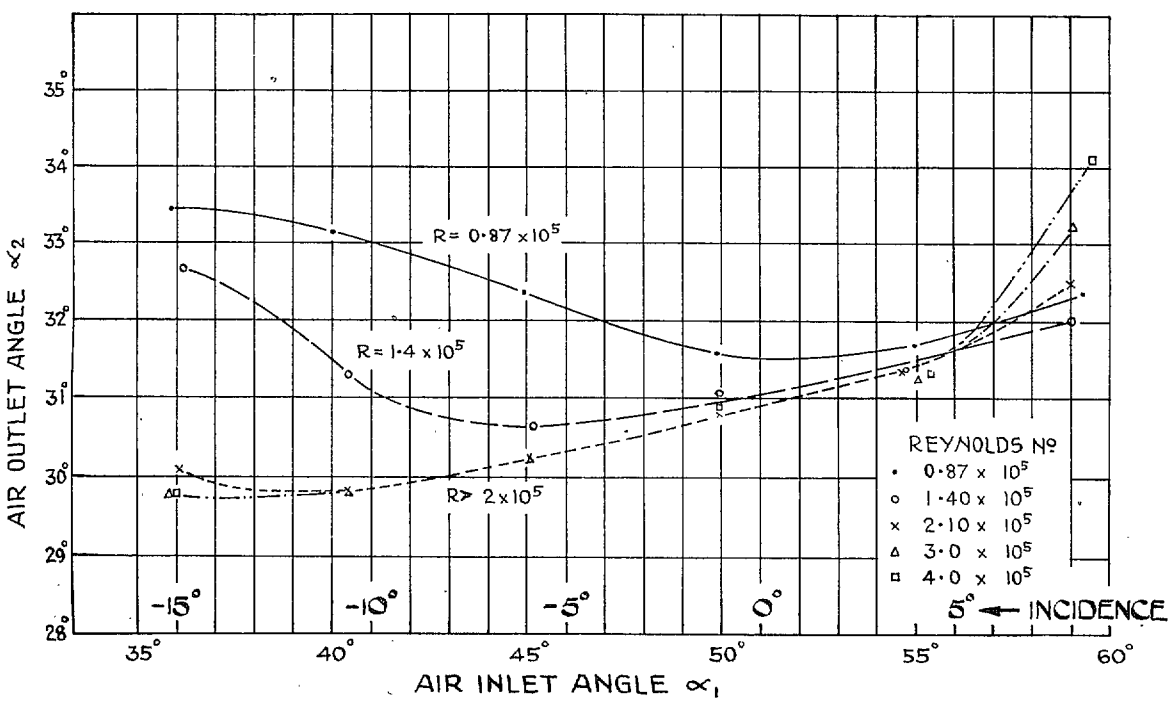

FIG. 16. Effect of Reynolds number on α_1 and α_2. 30-deg camber cascade.

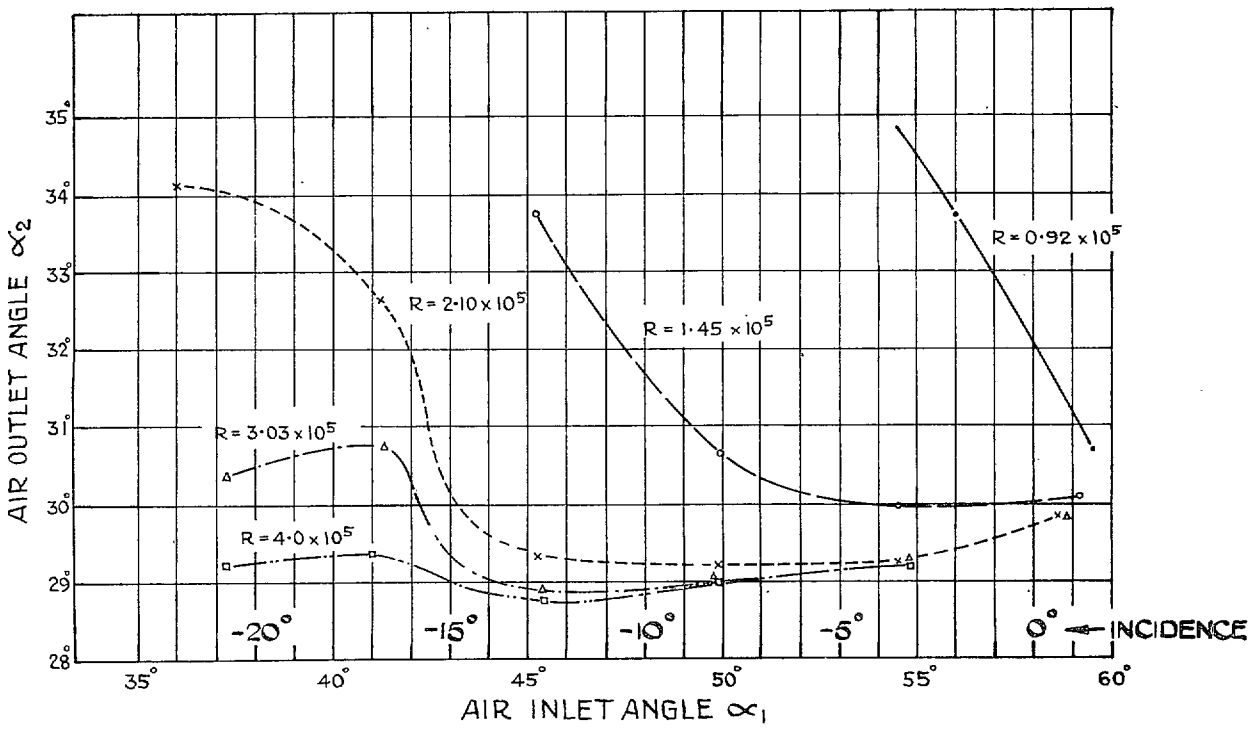

FIG. 17. Effect of Reynolds number on α_1 and α_2. 40-deg camber cascade.

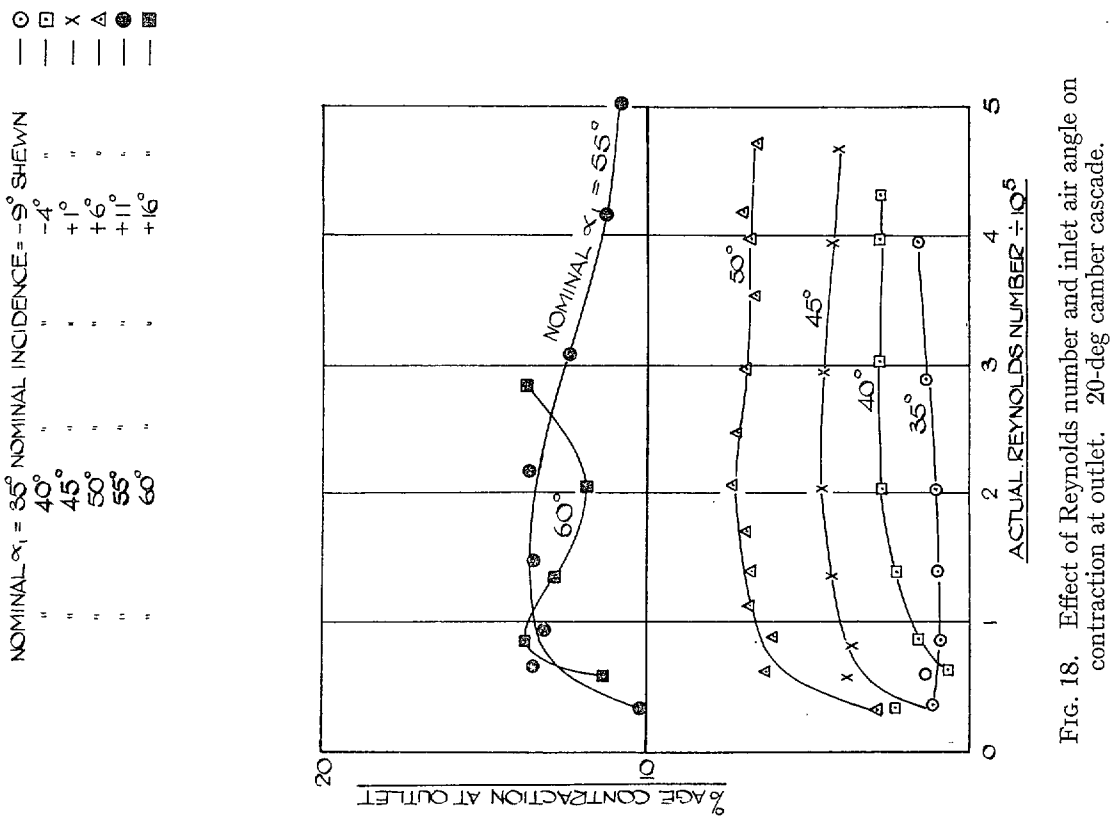

FIG. 18. Effect of Reynolds number and inlet air angle on contraction at outlet. 20-deg camber cascade.

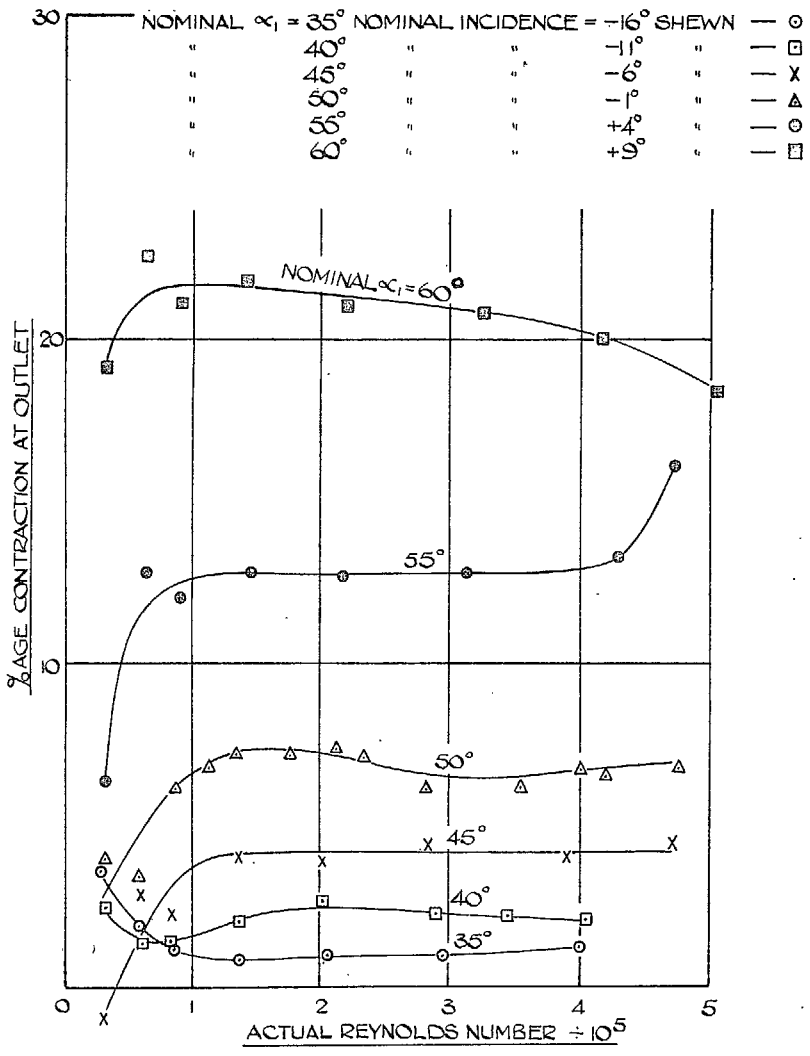

FIG. 19. Effect of Reynolds number and inlet air angle on contraction at outlet. 30-deg camber cascade.

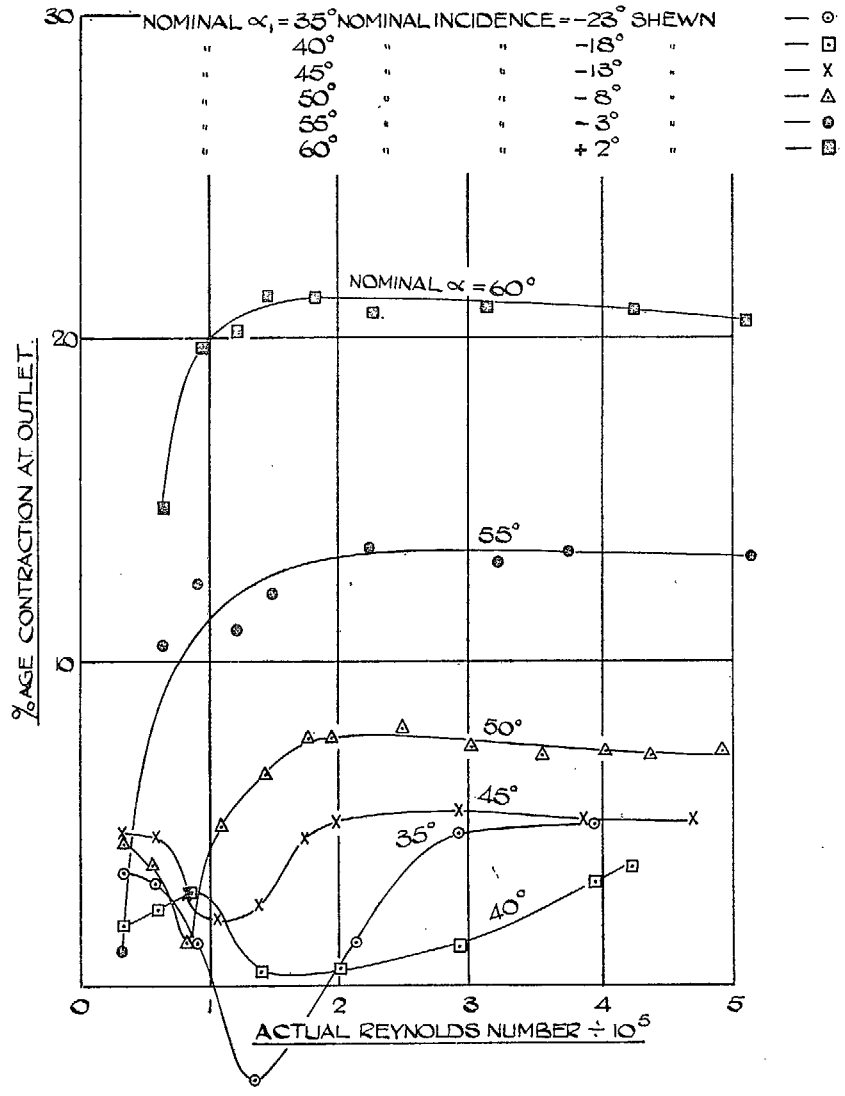

FIG. 20. Effect of Reynolds number and inlet air angle on contraction at outlet. 40-deg camber cascade.

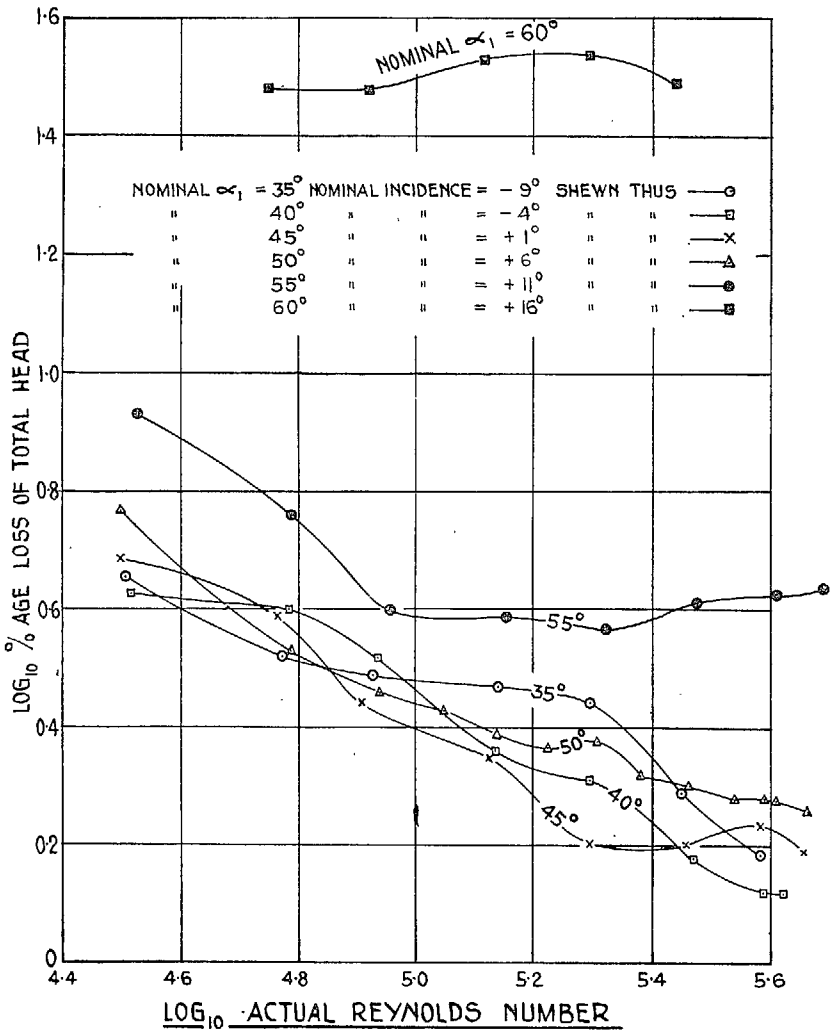

FIG. 21. Effect of Reynolds number and inlet air angle on loss of total head. 20-deg camber cascade.

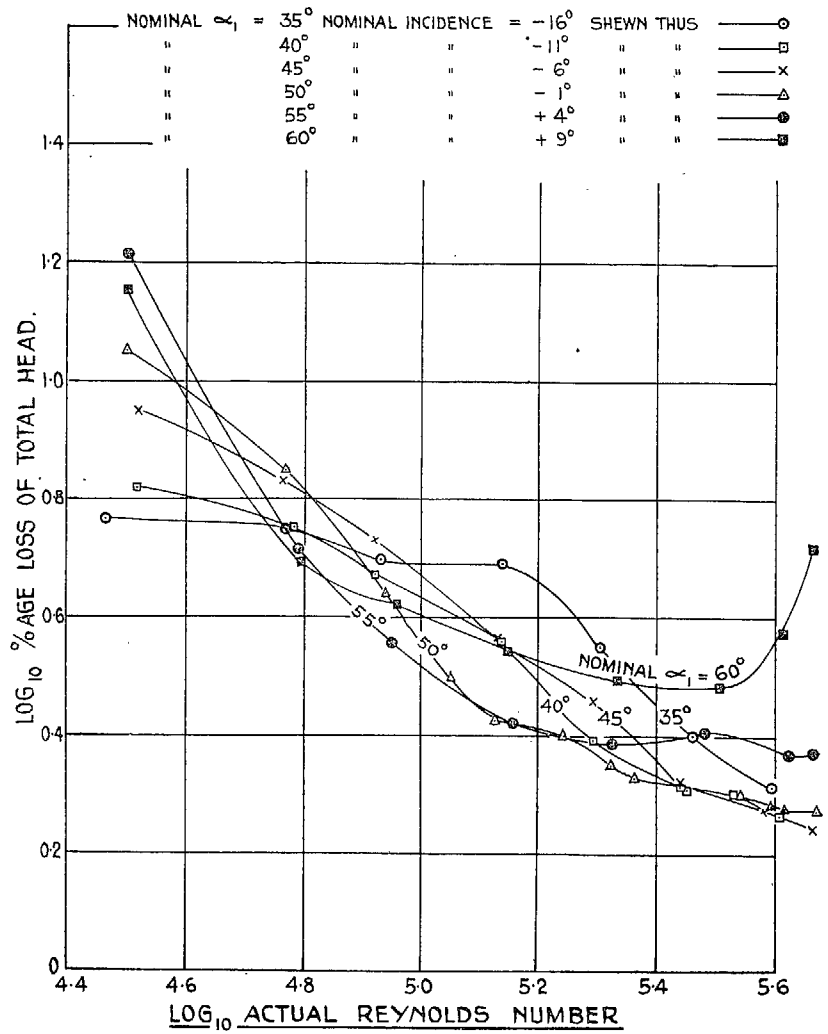

FIG. 22. Effect of Reynolds number and inlet air angle on loss of total head. 30-deg camber cascade.

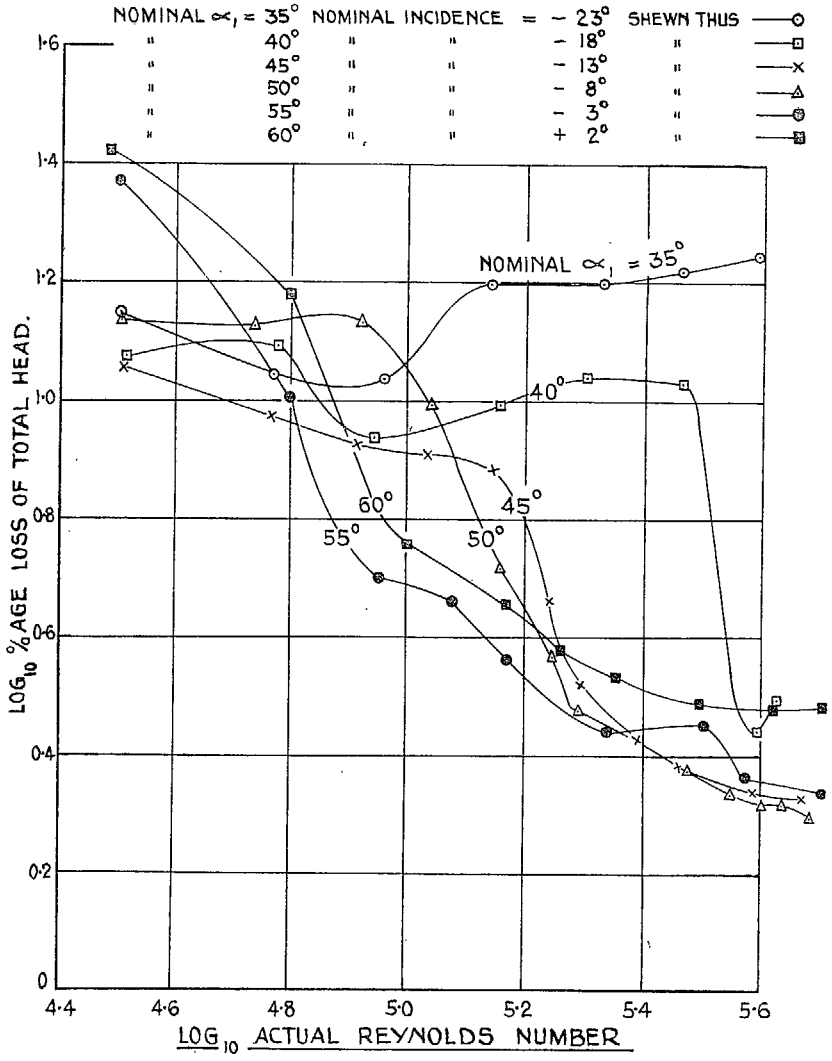

FIG. 23. Effect of Reynolds number and inlet air angle on loss of total head. 40-deg camber cascade.

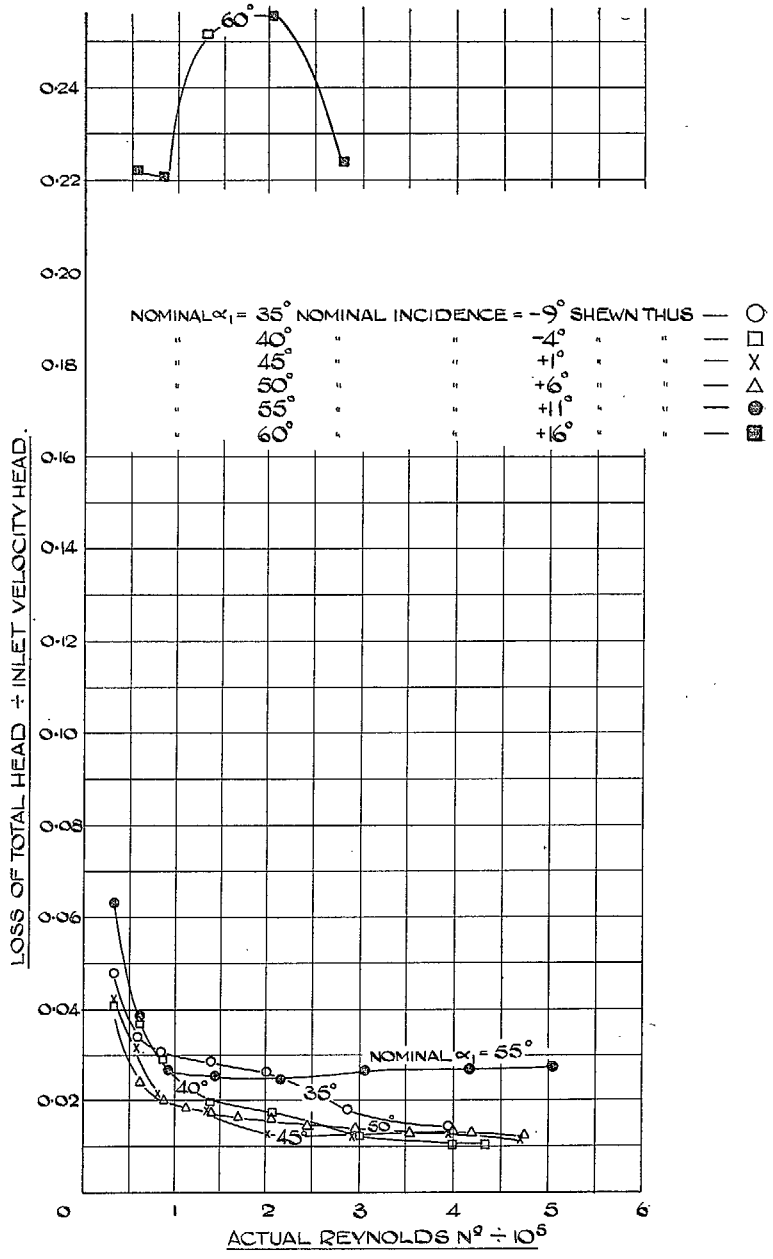

FIG. 24. Effect of Reynolds number and inlet air angle on loss of total head. 20-deg camber cascade.

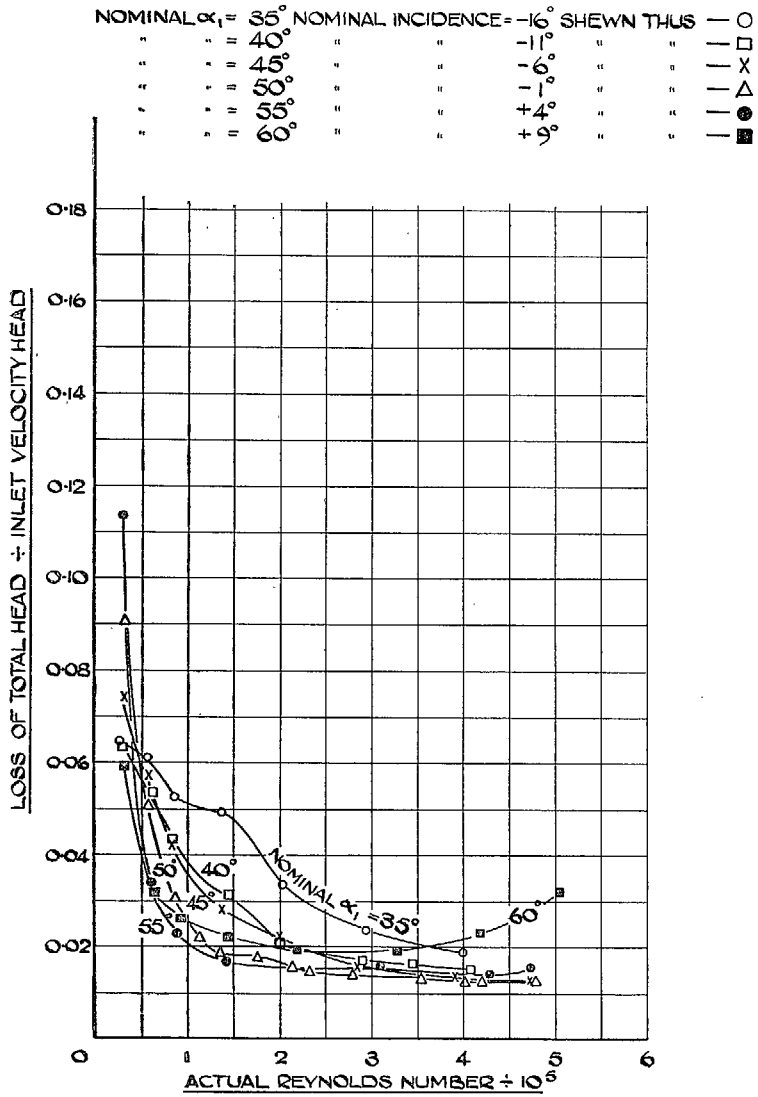

FIG. 25. Effect of Reynolds number and inlet air angle on loss of total head. 30-deg camber cascade.

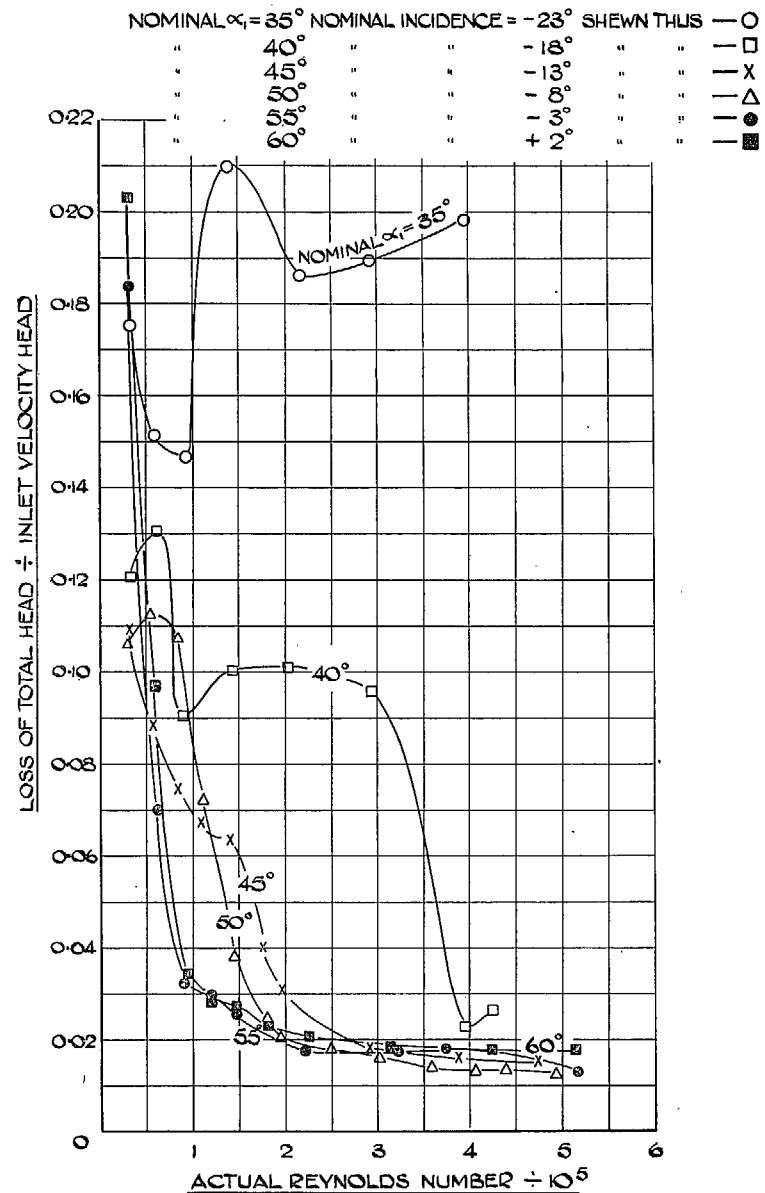

FIG. 26. Effect of Reynolds number and inlet air angle on loss of total head. 40-deg camber cascade.

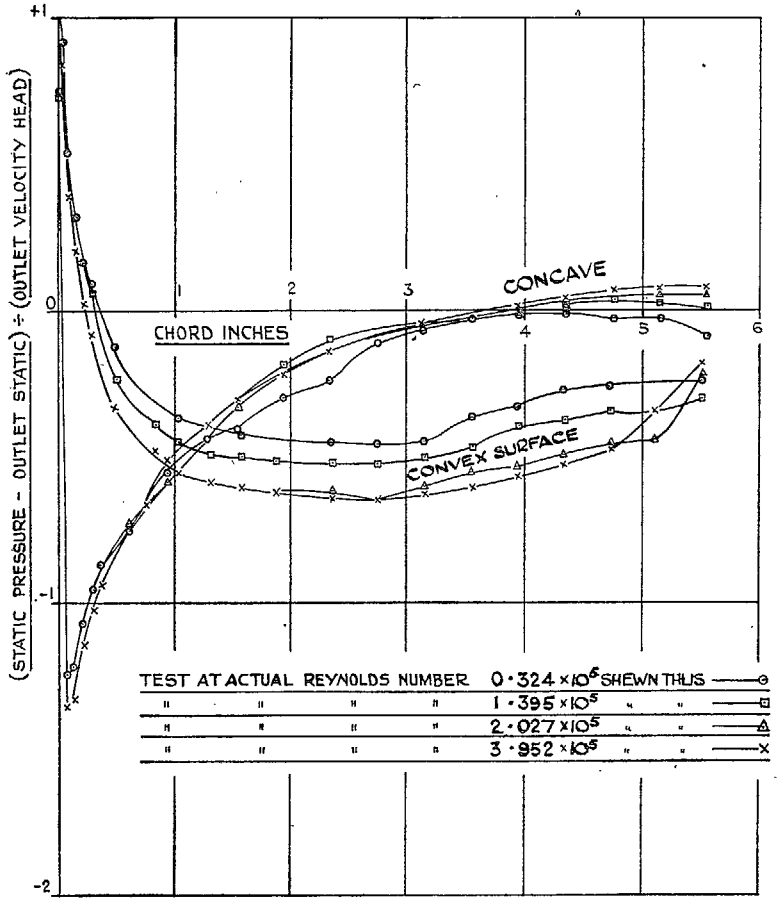

FIG. 27. Pressure distribution around central cross-section of middle blade. 20-deg camber cascade. Nominal $\alpha_1 = 35$ deg. Incidence = — 9 deg.

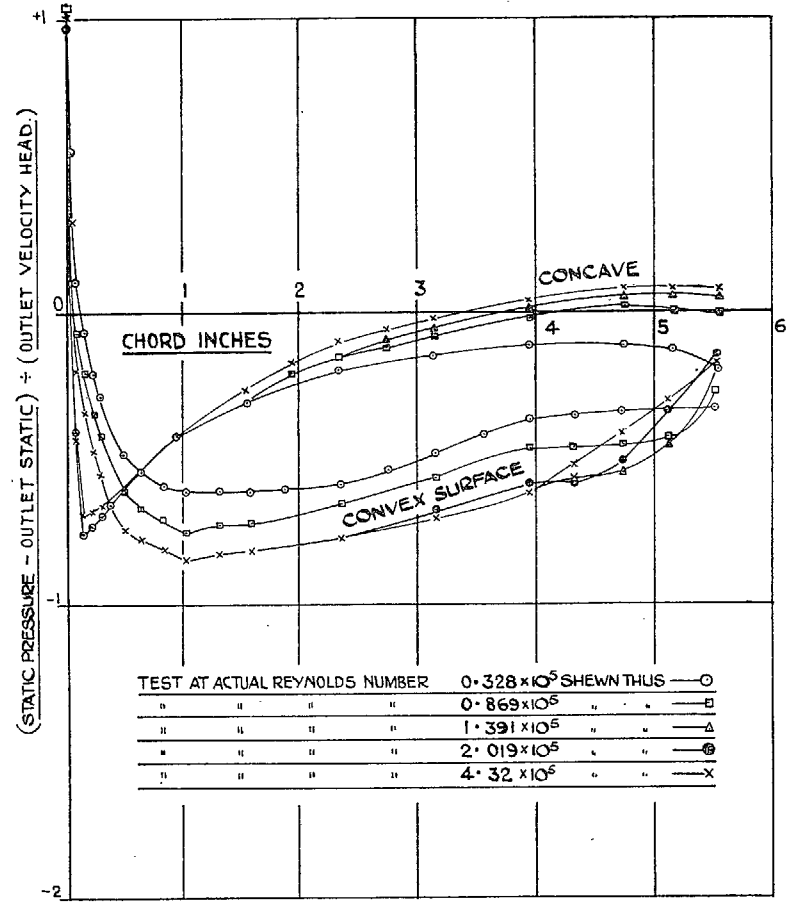

FIG 28. Pressure distribution around central cross-section of middle blade. 20-deg camber cascade. Nominal $\alpha_1 = 40$ deg. Incidence = — 4 deg.

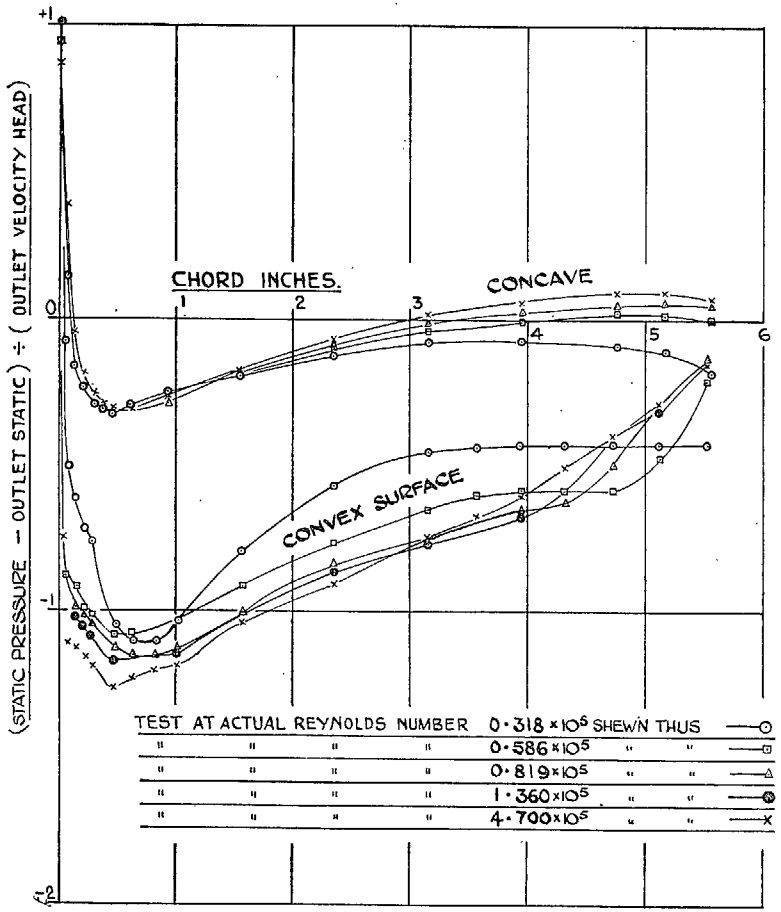

FIG. 29. Pressure distribution around central cross-section of middle blade. 20-deg camber cascade. Nominal $\alpha_1 = 45$ deg. Incidence $= +1$ deg.

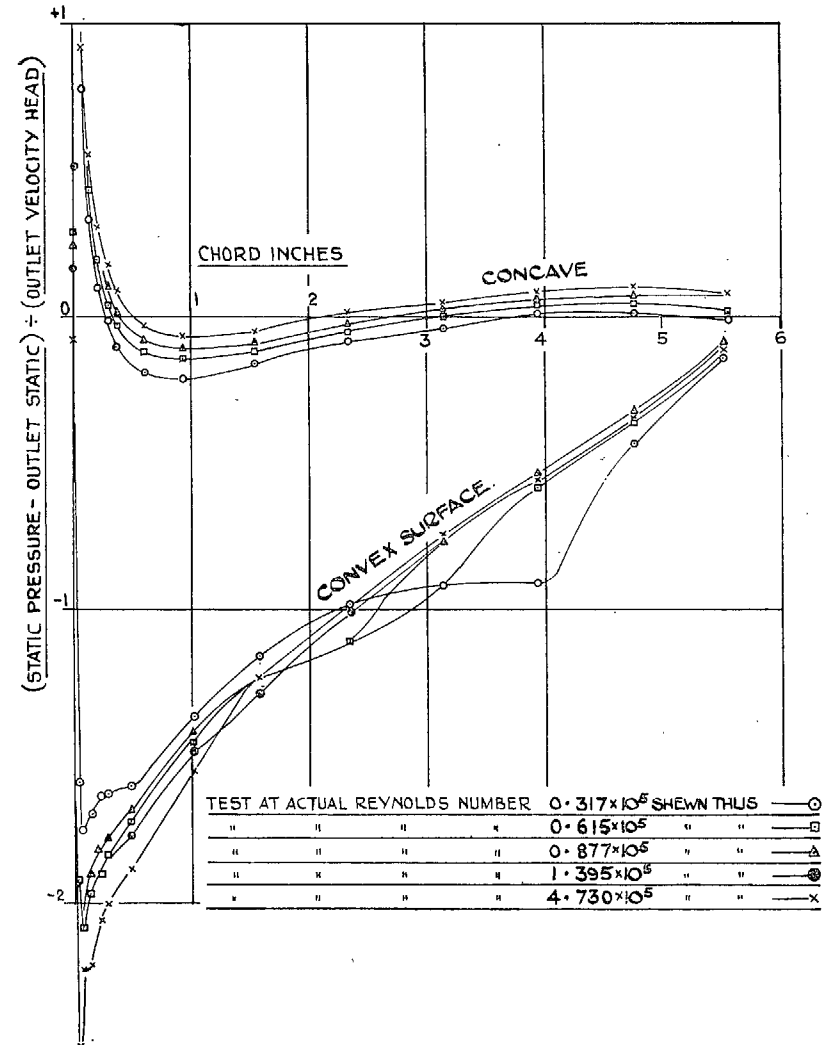

FIG. 30. Pressure distribution around central cross-section of middle blade. 20-deg camber cascade. Nominal $\alpha_1 = 50$ deg. Incidence $= +6$ deg.

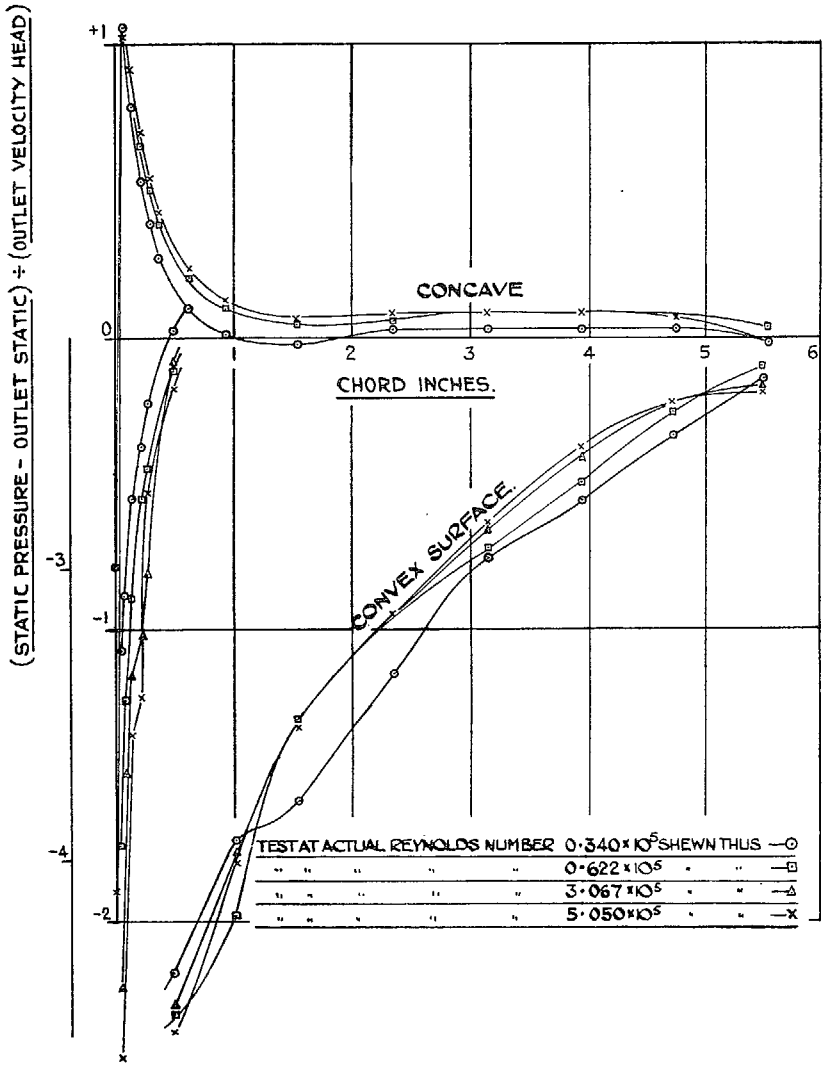

FIG. 31. Pressure distribution around central cross-section of middle blade. 20-deg camber cascade. Nominal $\alpha_1 = 55$ deg. Incidence = + 11 deg.

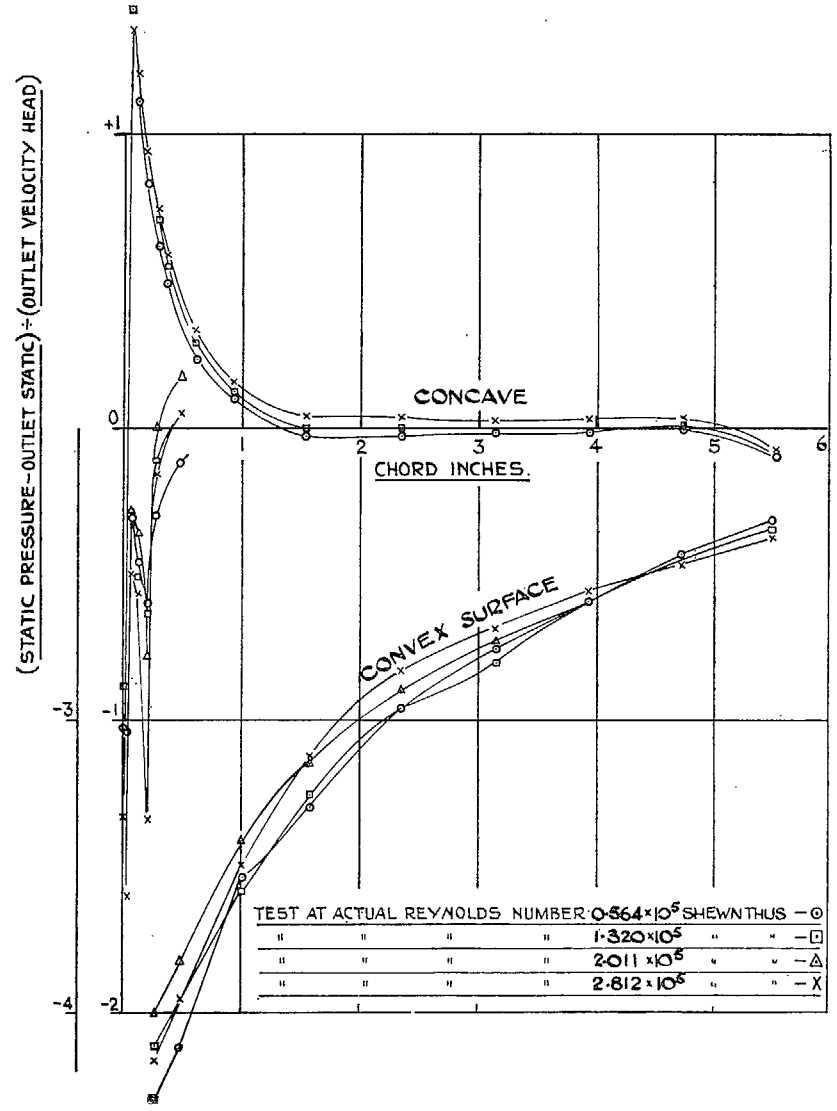

FIG. 32. Pressure distribution around central cross-section of middle blade. 20-deg camber cascade. Nominal $\alpha_1 = 60$ deg. Incidence = + 16 deg.

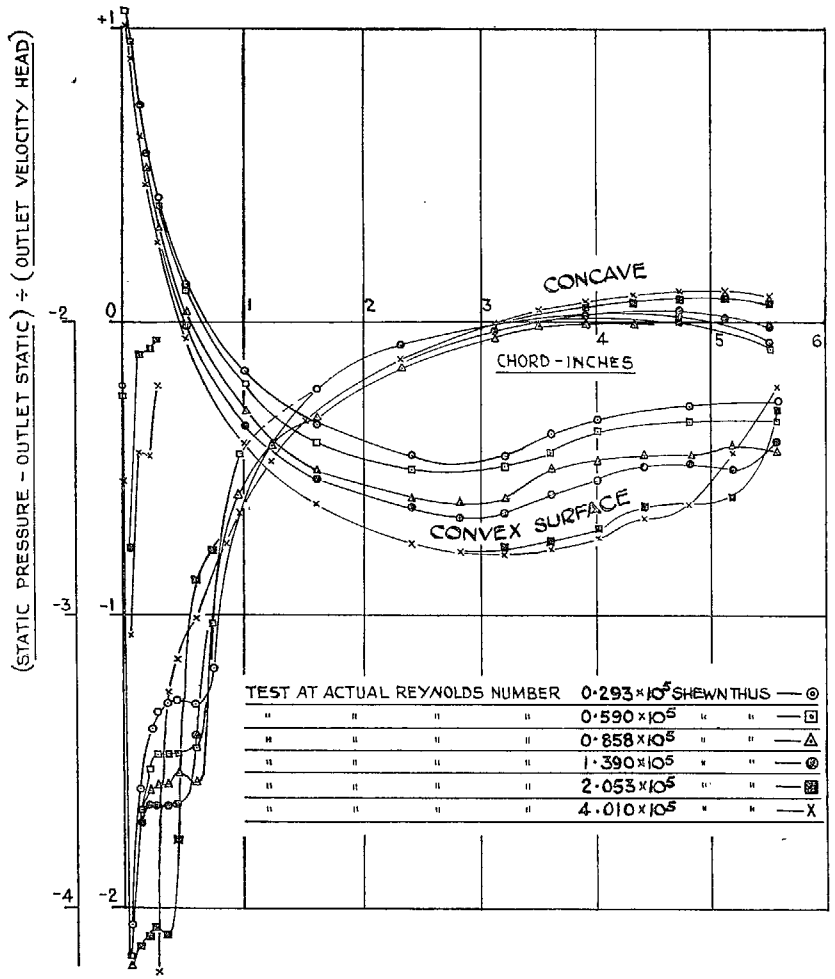

FIG. 33. Pressure distribution around central cross-section of middle blade. 30-deg camber cascade. Nominal $\alpha_1 = 35$ deg. Incidence = — 16 deg.

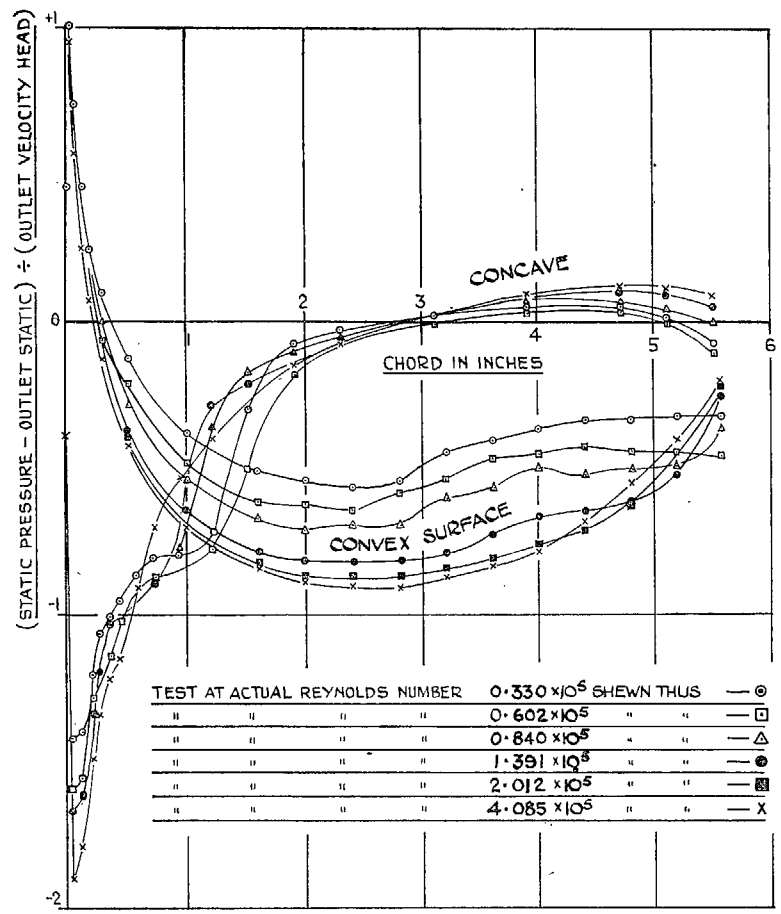

FIG. 34. Pressure distribution around central cross-section of middle blade. 30-deg camber cascade. Nominal $\alpha_1 = 40$ deg. Incidence = — 11 deg.

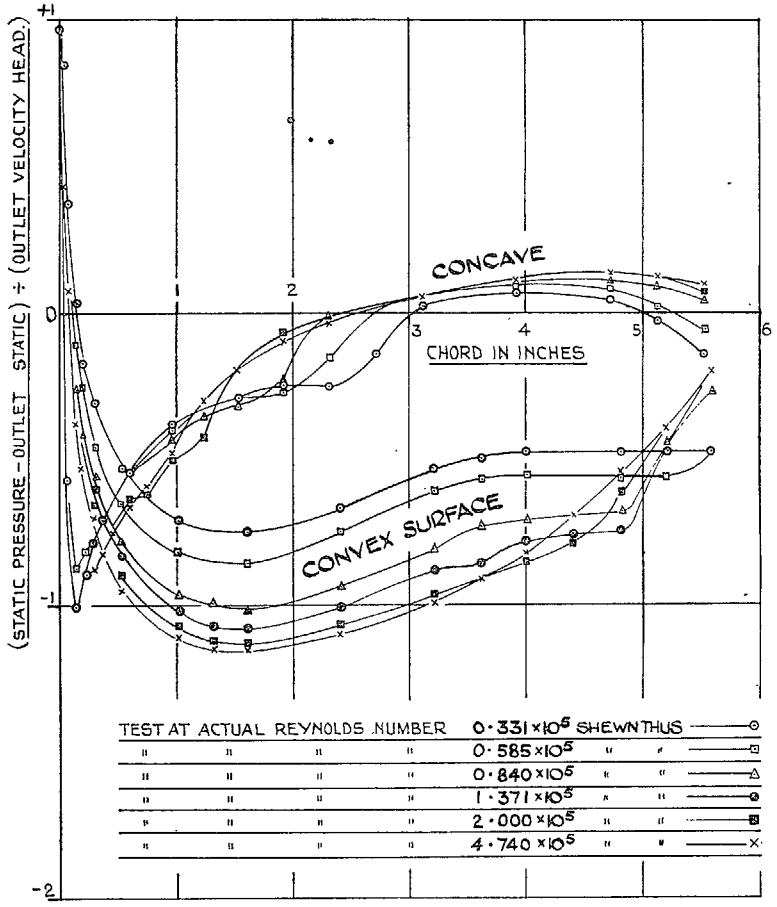

FIG. 35. Pressure distribution around central cross-section of middle blade. 30-deg camber cascade. Nominal $\alpha_1 = 45$ deg. Incidence = — 6 deg.

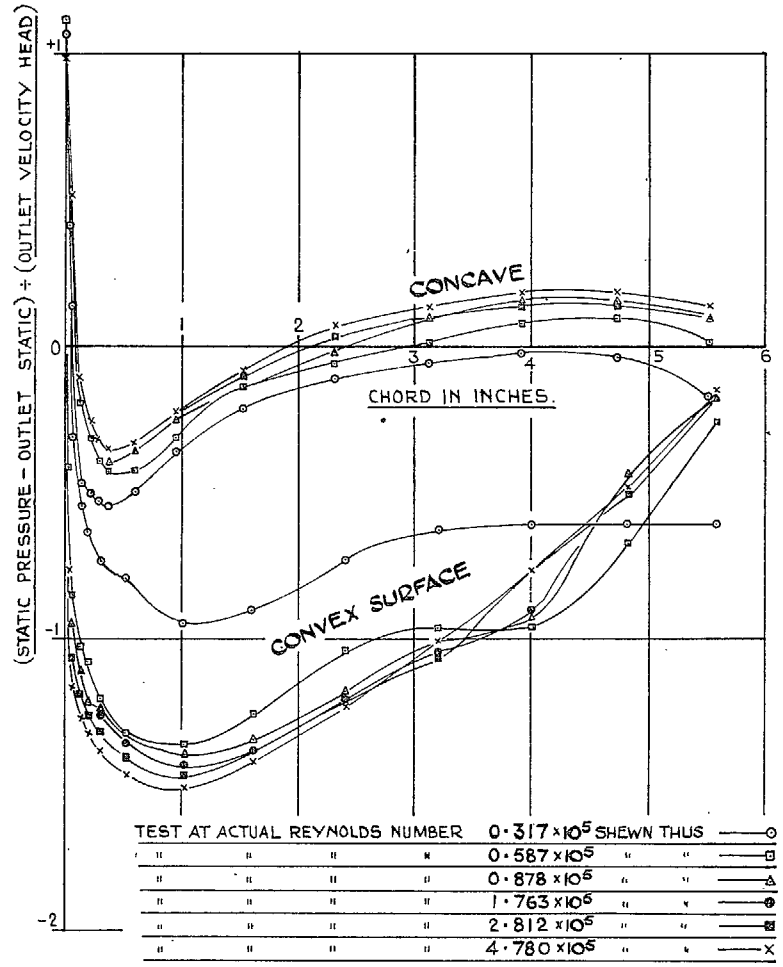

FIG. 36. Pressure distribution around central cross-section of middle blade. 30-deg camber cascade. Nominal $\alpha_1 = 50$ deg. Incidence = — 1 deg.

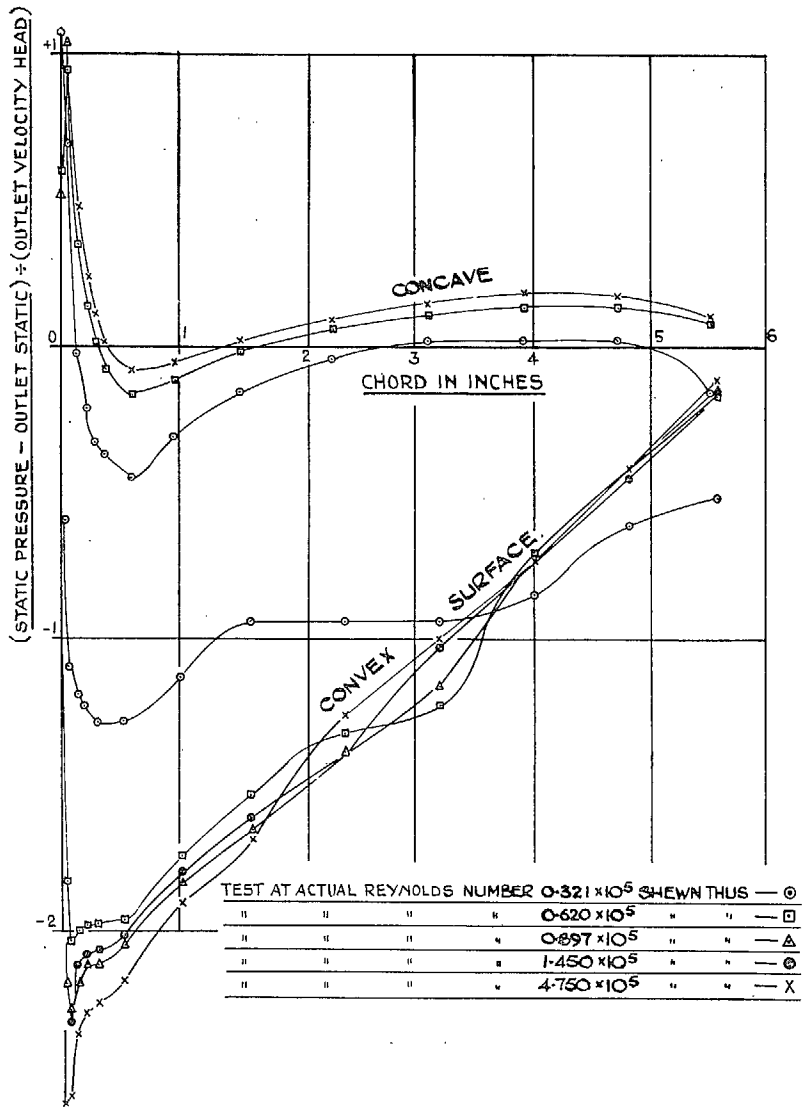

FIG. 37. Pressure distribution around central cross-section of middle blade. 30-deg camber cascade. Nominal $\alpha_1 = 55$ deg. Incidence = + 4 deg.

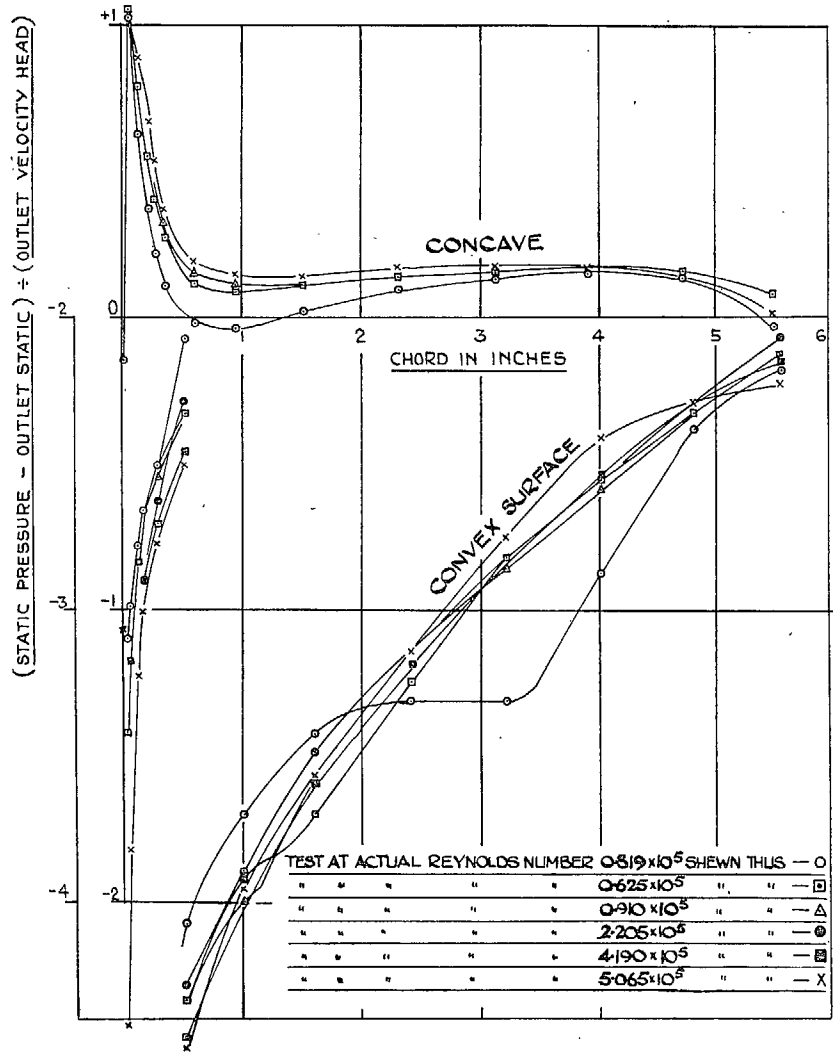

FIG. 38. Pressure distribution around central cross-section of middle blade. 30-deg camber cascade. Nominal $\alpha_1 = 60$ deg. Incidence = + 9 deg.

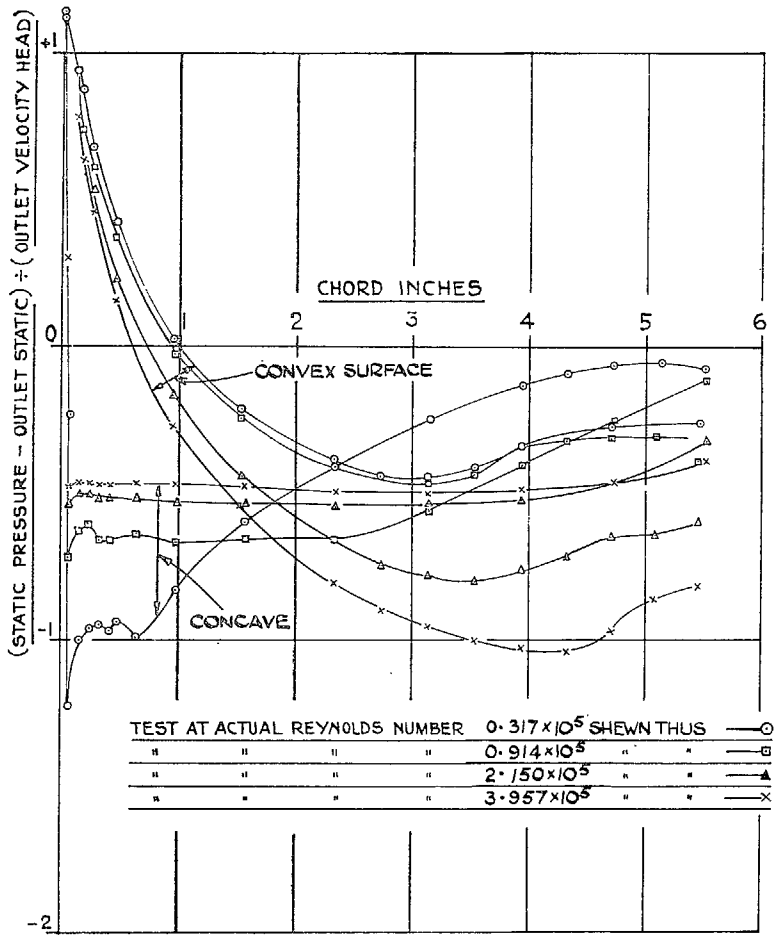

FIG. 39. Pressure distribution around central cross-section of middle blade. 40-deg camber cascade. Nominal $\alpha_1 = 35$ deg. Incidence = — 23 deg.

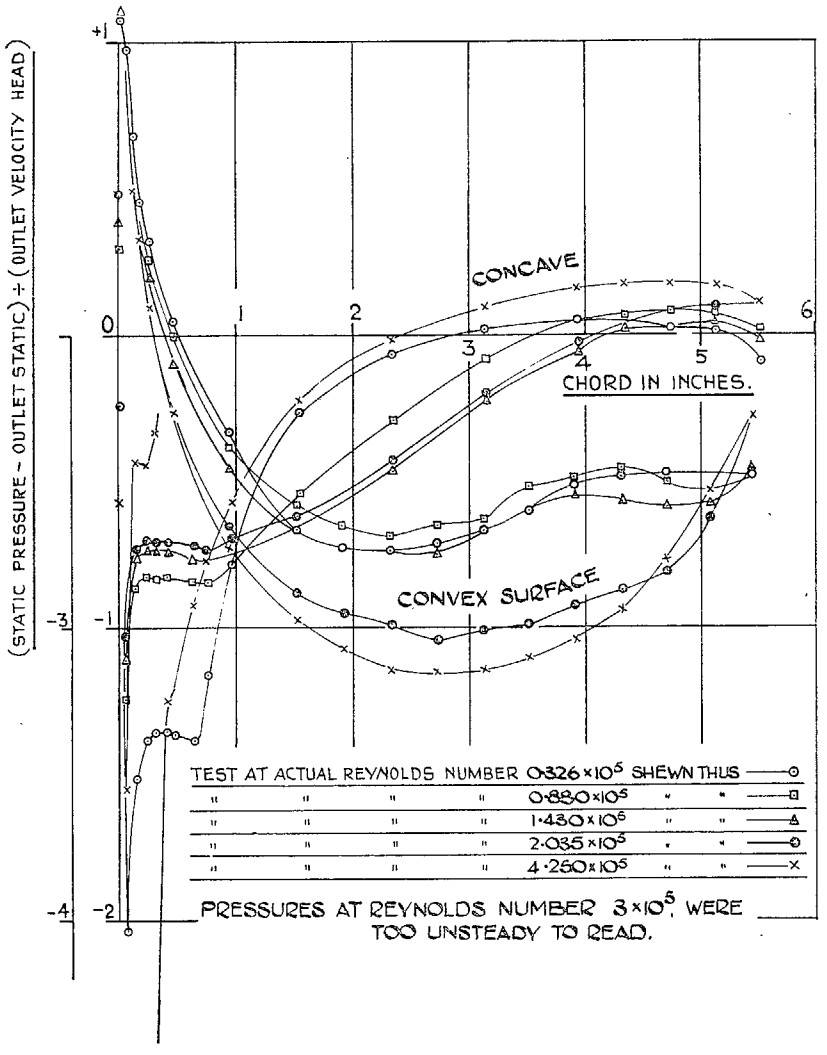

FIG. 40. Pressure distribution around central cross-section of middle blade. 40-deg camber cascade. Nominal $\alpha_1 = 40$ deg. Incidence = — 18 deg.

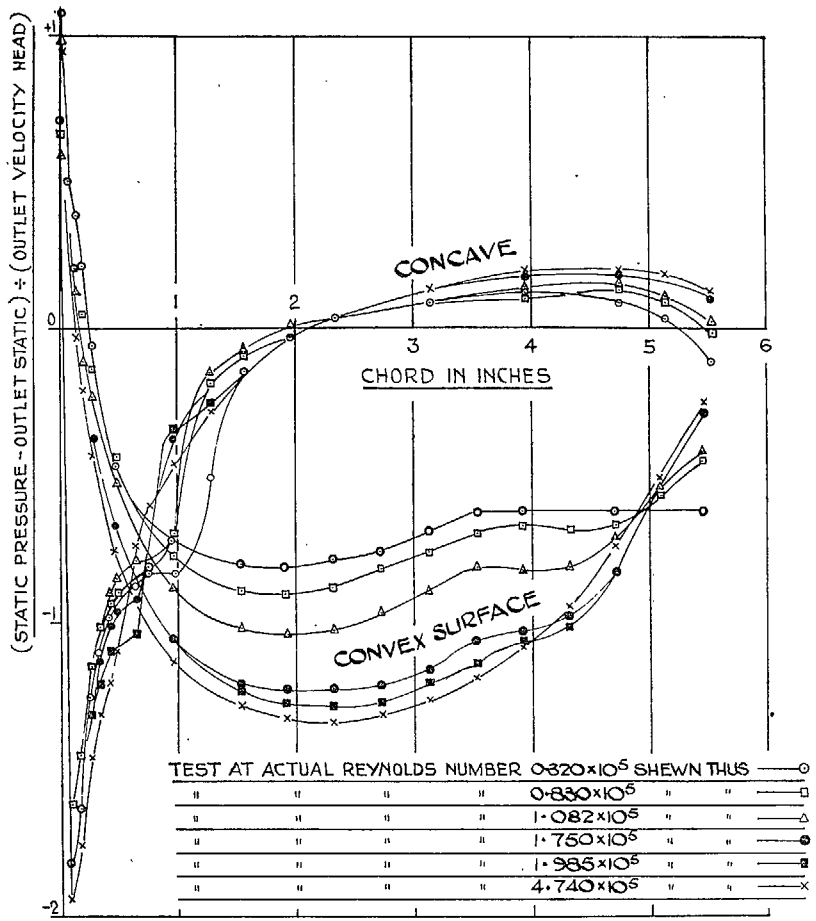

FIG. 41. Pressure distribution around central cross-section of middle blade. 40-deg camber cascade. Nominal $\alpha_1 = 45$ deg. Incidence = — 13 deg.

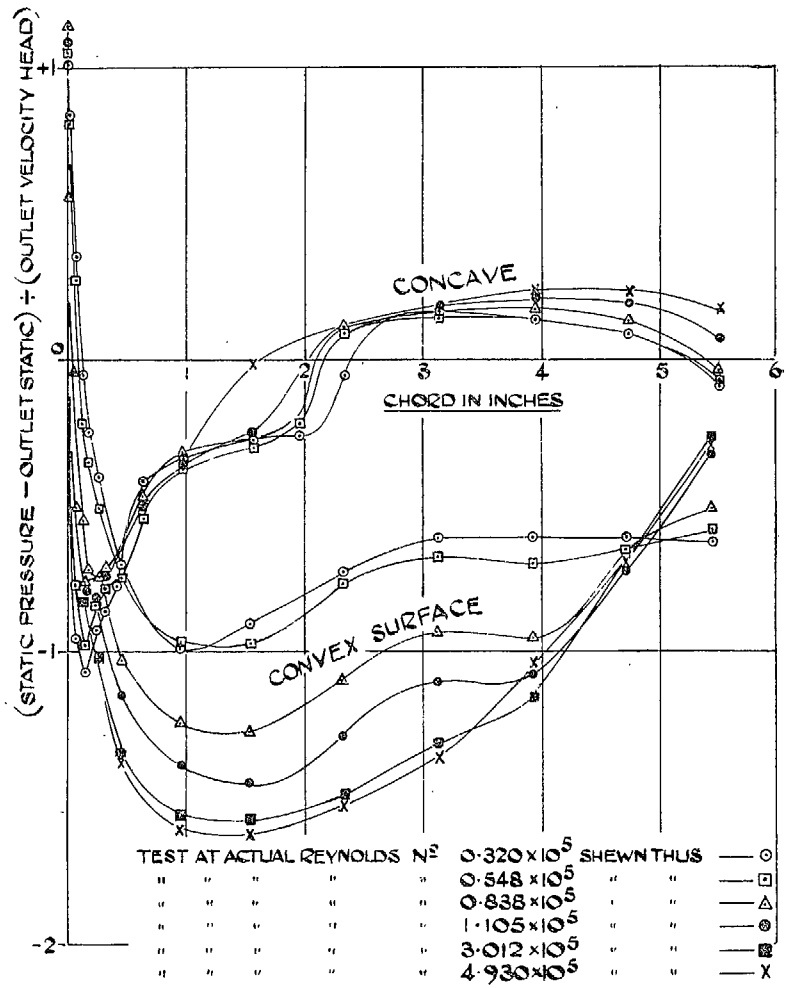

FIG. 42. Pressure distribution around central cross-section of middle blade. 40-deg camber cascade. Nominal $\alpha_1 = 50$ deg. Incidence = — 8 deg.

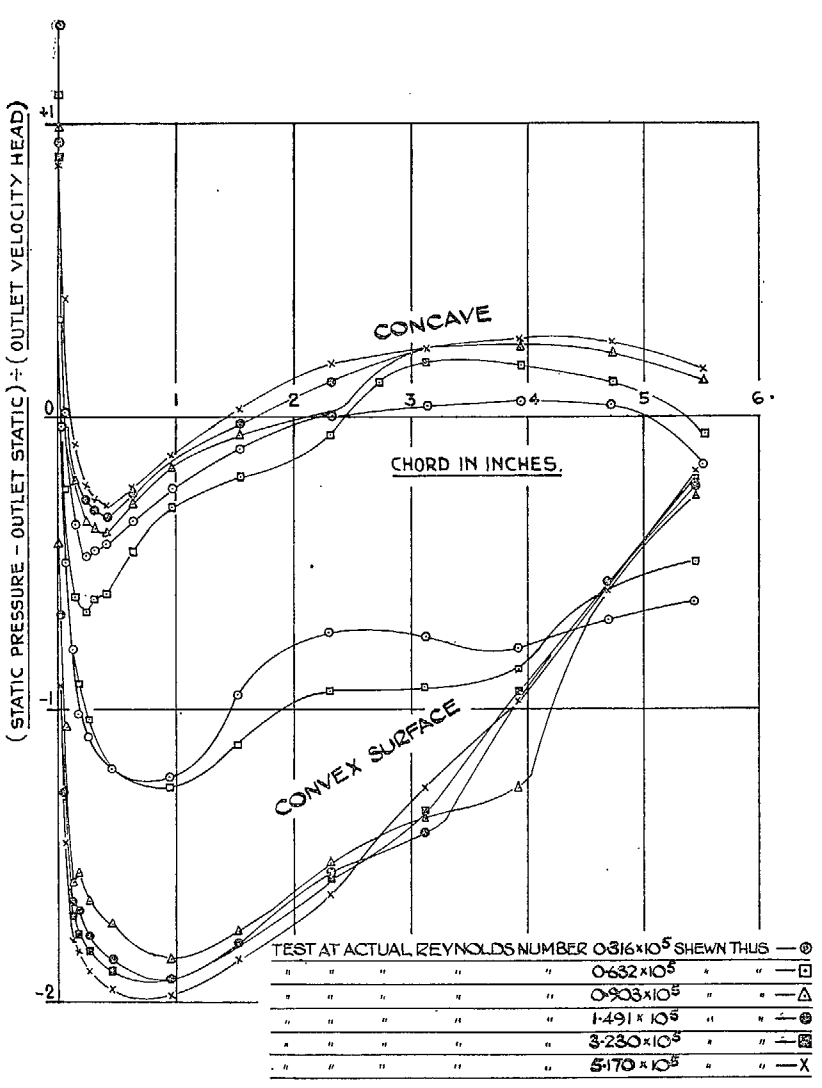

FIG. 43. Pressure distribution around central cross-section of middle blade. 40-deg camber cascade. Nominal $\alpha_1 = 55$ deg. Incidence = — 3 deg.

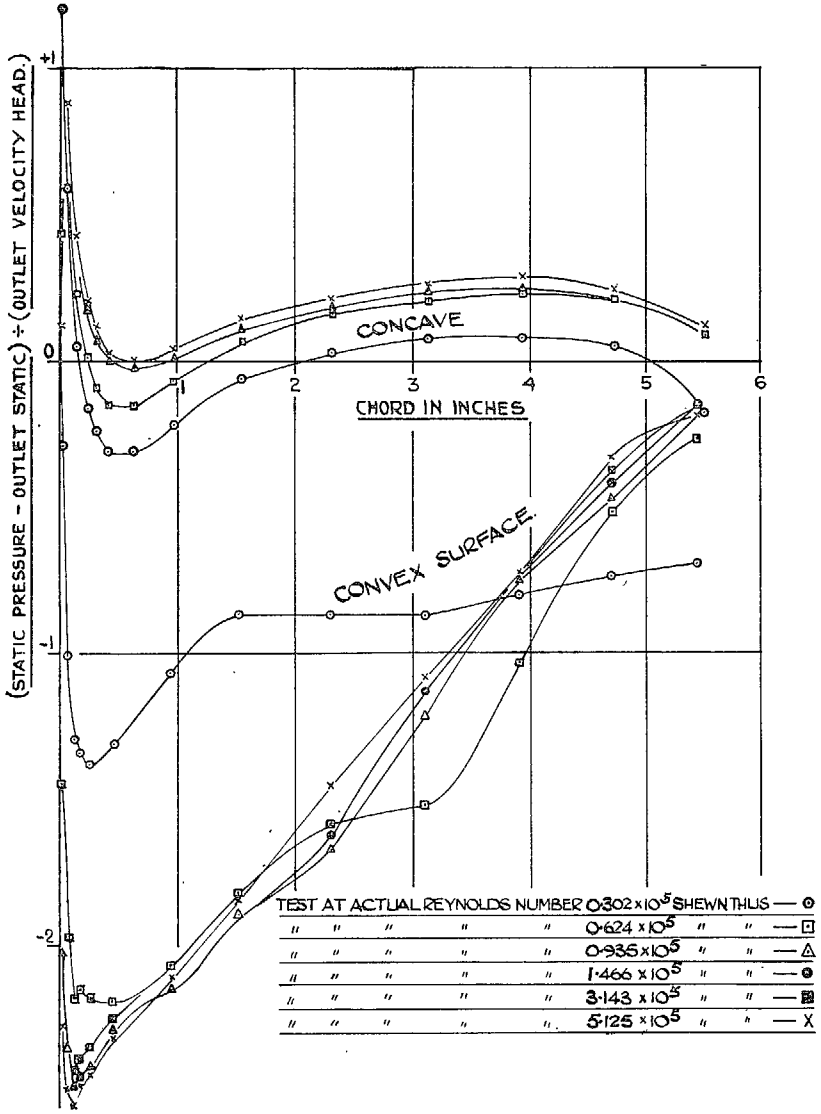

FIG. 44. Pressure distribution around central cross-section of middle blade. 40-deg camber cascade. Nominal $\alpha_1 = 60$ deg. Incidence = + 2 deg.

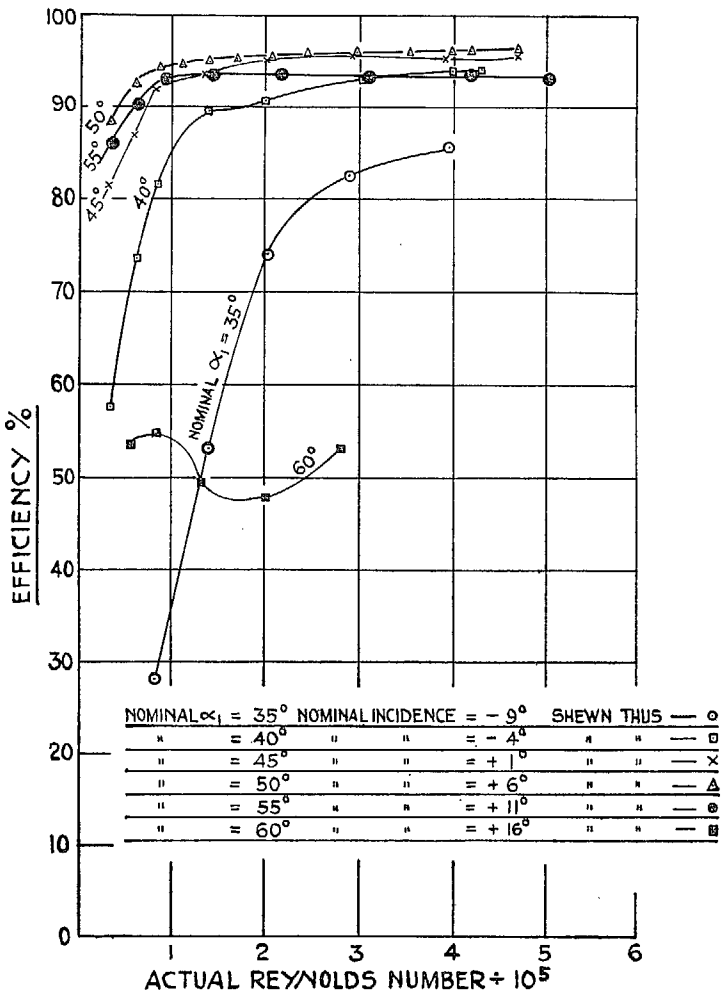

FIG. 45. Effect of Reynolds number and inlet air angle on efficiency. 20-deg camber cascade.

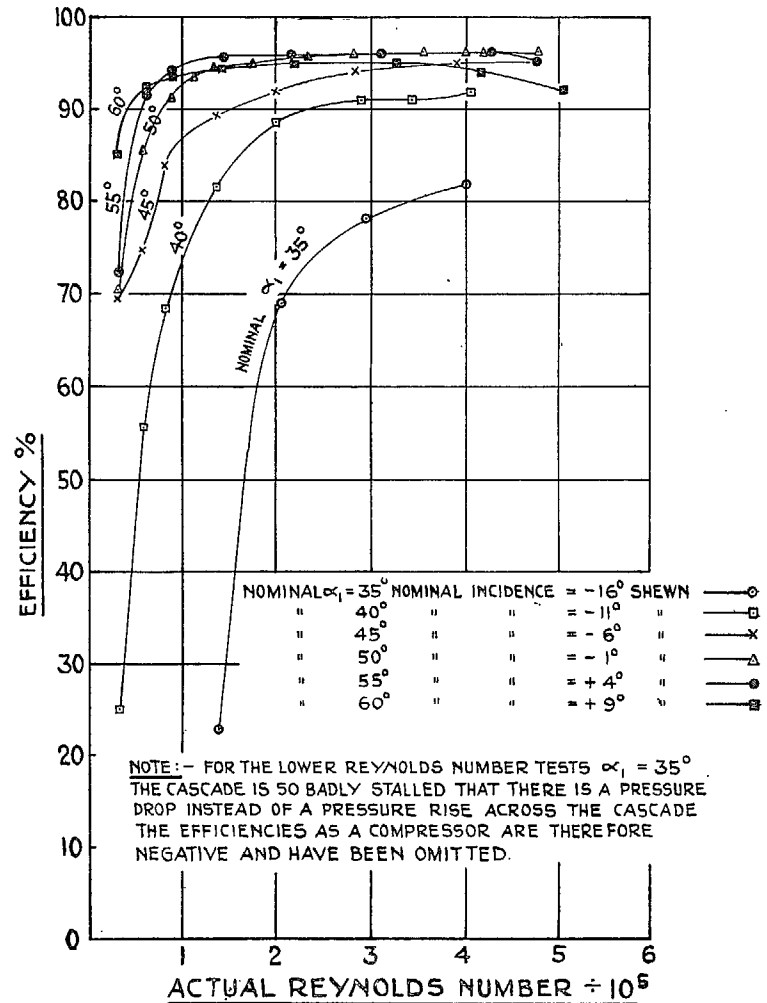

FIG. 46. Effect of Reynolds number and inlet air angle on efficiency. 30-deg camber cascade.

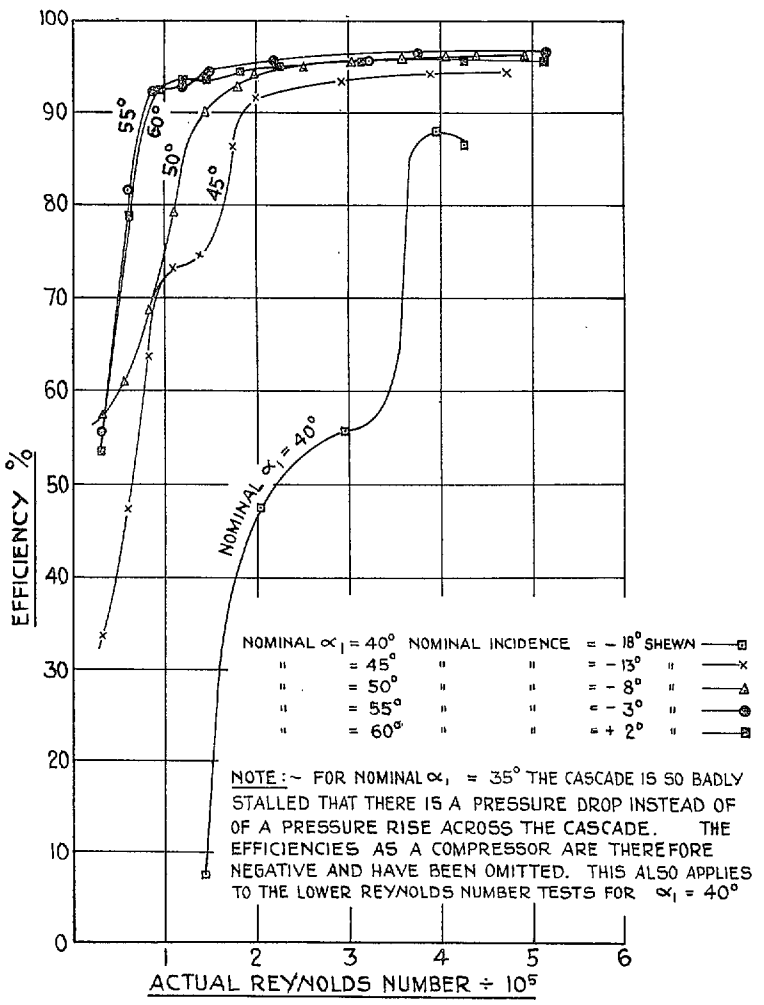

FIG. 47. Effect of Reynolds number and inlet air angle on efficiency. 40-deg camber cascade.

(2656) Wt. 18/9296 K.7 6/56 Hw. PRINTED IN GREAT BRITAIN

Publications of the Aeronautical Research Council

ANNUAL TECHNICAL REPORTS OF THE AERONAUTICAL RESEARCH COUNCIL (BOUND VOLUMES)

1938 Vol. I. Aerodynamics General, Performance, Airscrews. 50*s*. (51*s*. 8*d*.)
Vol. II. Stability and Control, Flutter, Structures, Seaplanes, Wind Tunnels, Materials. 30*s*. (31*s*. 8*d*.)

1939 Vol. I. Aerodynamics General, Performance, Airscrews, Engines. 50*s*. (51*s*. 8*d*.)
Vol. II. Stability and Control, Flutter and Vibration, Instruments, Structures, Seaplanes, etc. 63*s*. (64*s*. 8*d*.)

1940 Aero and Hydrodynamics, Aerofoils, Airscrews, Engines, Flutter, Icing, Stability and Control, Structures, and a miscellaneous section. 50*s*. (51*s*. 8*d*.)

1941 Aero and Hydrodynamics, Aerofoils, Airscrews, Engines, Flutter, Stability and Control, Structures. 63*s*. (64*s*. 8*d*.)

1942 Vol. I. Aero and Hydrodynamics, Aerofoils, Airscrews, Engines. 75*s*. (76*s*. 8*d*.)
Vol. II. Noise, Parachutes, Stability and Control, Structures, Vibration, Wind Tunnels. 47*s*. 6*d*. (49*s*. 2*d*.)

1943 Vol. I. Aerodynamics, Aerofoils, Airscrews. 80*s*. (81*s*. 8*d*.)
Vol. II. Engines, Flutter, Materials, Parachutes, Performance, Stability and Control, Structures. 90*s*. (91*s*. 11*d*.)

1944 Vol. I. Aero and Hydrodynamics, Aerofoils, Aircraft, Airscrews, Controls. 84*s*. (86*s*. 9*d*.)
Vol. II. Flutter and Vibration, Materials, Miscellaneous, Navigation, Parachutes, Performance, Plates and Panels, Stability, Structures, Test Equipment, Wind Tunnels. 84*s*. (86*s*. 9*d*.)

Annual Reports of the Aeronautical Research Council—

1933–34	1*s*. 6*d*. (1*s*. 8½*d*.)	1937	2*s*. (2*s*. 2½*d*.)
1934–35	1*s*. 6*d*. (1*s*. 8½*d*.)	1938	1*s*. 6*d*. (1*s*. 8½*d*.)
April 1, 1935 to Dec. 31, 1936	4*s*. (4*s*. 5½*d*.)	1939–48	3*s*. (3*s*. 3½*d*.)

Index to all Reports and Memoranda published in the Annual Technical Reports, and separately—

April, 1950 - - - - R. & M. No. 2600 2*s*. 6*d*. (2*s*. 7½*d*.)

Author Index to all Reports and Memoranda of the Aeronautical Research Council—

1909–January, 1954. R. & M. No. 2570 15*s*. (15*s*. 5½*d*.)

Indexes to the Technical Reports of the Aeronautical Research Council—

December 1, 1936 — June 30, 1939	R. & M. No. 1850	1*s*. 3*d*. (1*s*. 4½*d*.)
July 1, 1939 — June 30, 1945	R. & M. No. 1950	1*s*. (1*s*. 1½*d*.)
July 1, 1945 — June 30, 1946	R. & M. No. 2050	1*s*. (1*s*. 1½*d*.)
July 1, 1946 — December 31, 1946	R. & M. No. 2150	1*s*. 3*d*. (1*s*. 4½*d*.)
January 1, 1947 — June 30, 1947	R. & M. No. 2250	1*s*. 3*d*. (1*s*. 4½*d*.)

Published Reports and Memoranda of the Aeronautical Research Council—

Between Nos. 2251–2349	R. & M. No. 2350	1*s*. 9*d*. (1*s*. 10½*d*.)
Between Nos. 2351–2449	R. & M. No. 2450	2*s*. (2*s*. 1½*d*.)
Between Nos. 2451–2549	R. & M. No. 2550	2*s*. 6*d*. (2*s*. 7½*d*.)
Between Nos. 2551–2649	R. & M. No. 2650	2*s*. 6*d*. (2*s*. 7½*d*.)

Prices in brackets include postage

HER MAJESTY'S STATIONERY OFFICE

York House, Kingsway, London W.C.2; 423 Oxford Street, London W.1 (Post Orders: P.O. Box 569, London S.E.1); 13a Castle Street, Edinburgh 2; 39 King Street, Manchester 2; 2 Edmund Street, Birmingham 3; 109 St. Mary Street, Cardiff; Tower Lane, Bristol, 1; 80 Chichester Street, Belfast, *or through any bookseller*

S.O. Code No. 23-2919